Design of photonic crystals and binary supergratings using Boolean particle swarm optimization

by

Farzaneh Afshinmanesh
B.Sc., University of Tehran, 2006

A Thesis Submitted in Partial Fulfillment of the
Requirements for the Degree of

Master of Applied Science

in the Department of Electrical and Computer Engineering

University of Victoria

Design of photonic crystals and binary supergratings using Boolean particle swarm optimization

by

Farzaneh Afshinmanesh
B.Sc., University of Tehran, 2006

Supervisory Committee

Prof. Poman P.M. So, Co-Supervisor (ECE Dept.)

Prof. Reuven Gordon, Co-Supervisor (ECE Dept.)

Prof. Jens H. Weber-Jahnke, Outside Member (ECS Dept.)

Supervisory Committee

Prof. Poman P.M. So, Co-Supervisor (ECE Dept.)

Prof. Reuven Gordon, Co-Supervisor (ECE Dept.)

Prof. Jens H. Weber-Jahnke, Outside Member (ECS Dept.)

Abstract

Photonic crystals (PCs) and binary supergratings (BSGs) with large refractive index steps are promising structures for designing new compact optical devices. This thesis presents an inverse design tool in these two important areas of photonics. The tool consists of an optimization module and a simulation engine. Due to the binary nature of PCs and BSGs, Boolean particle swarm optimization (Boolean PSO), a recently proposed binary stochastic optimization algorithm, is used in the optimization module. The simulation engine, on the other hand, is chosen according to the structure to be modeled. The proposed inverse design tool has been used to design a very low F-number photonic crystal lens and compact BSG filters for applications such as wavelength-division multiplexing, tunable lasers and intrachip optical networks. The inverse design tool allows designing optical filters with almost arbitrary wavelength filtering, in addition the proposed filters are more compact than previous demonstrations of BSG. Furthermore, it is found that Boolean PSO outperforms Genetic Algorithm (GA) as an optimization technique for use in the inverse design tool developed in this thesis.

Table of Contents

List of Figures

Chapter 1

Introduction

The increasing capability of computers in terms of computation speed and memory capacity accompanied by the advent of accurate simulation tools have opened a new road to engineering design named "inverse design". The capability of this type of design has been shown in various problems by designing devices with better functionalities in comparison to directly designed devices. In addition, inverse design has enabled researchers to obtain intricate structures which could not be designed with conventional methods. Inverse design procedures have been widely applied to engineering design problems and their use in various electromagnetic applications such as antennas [9, 10] and photonic crystals [11] has become widespread.

In inverse design methods, a functionality is considered and then a design is explored in the space of possible solutions to provide that functionality. Inverse design methods utilize a simulation tool to evaluate the performance of a possible design in addition to an optimization technique to improve the design, iteratively. Using an inverse design strategy makes it possible to design a system which has a close to desired behavior, without any prior knowledge of possible configurations. Evolutionary algorithms [12] are a popular class of stochastic optimization methods for finding global or close to global optimum points in ultra-large search spaces resulted from non-polynomial time problems.

Figure 1.1 shows the schematic representation of an inverse design process combining an evolutionary optimization technique with a simulation engine. The inverse design process starts with generating a set of random designs. The optimization goal is to find a design which provides a desired functionality. For each of the designs generated in the first step, its functionality is determined using a simulation engine. A fitness number is assigned to each design based on the difference between its functionality and the desired functionality. Higher fitness indicates better functionality of a design. The evolutionary algorithm creates a new set of designs based on the evaluated fitnesses in the first step. This iterative procedure continues until the best obtained design in an iteration satisfies the optimization goal. The best obtained design (the design with the best fitness) would be the final design.

Particle swarm optimization (PSO) [13] and genetic algorithms (GA) [14] are two popular classes of evolutionary algorithms that have been applied successfully in a variety of fields [15, 16] including electromagnetics [9, 17] and photonics [18, 19]. In comparison with GA, PSO is easier to understand and implement and its parameters have more straightforward effects on the optimization performance [9, 20, 21].

In this thesis, inverse design in two important areas of photonics, namely photonic crystals and binary supergratings are considered. These structures offer various promising optical devices because of their ability to efficiently control the propagation of light. Due to the the binary nature of these problems, a recently developed binary version of PSO called Boolean PSO [20, 21] is used as the optimization engine in design tools; the simulation engine in the design tool depends upon the structure to be modeled.

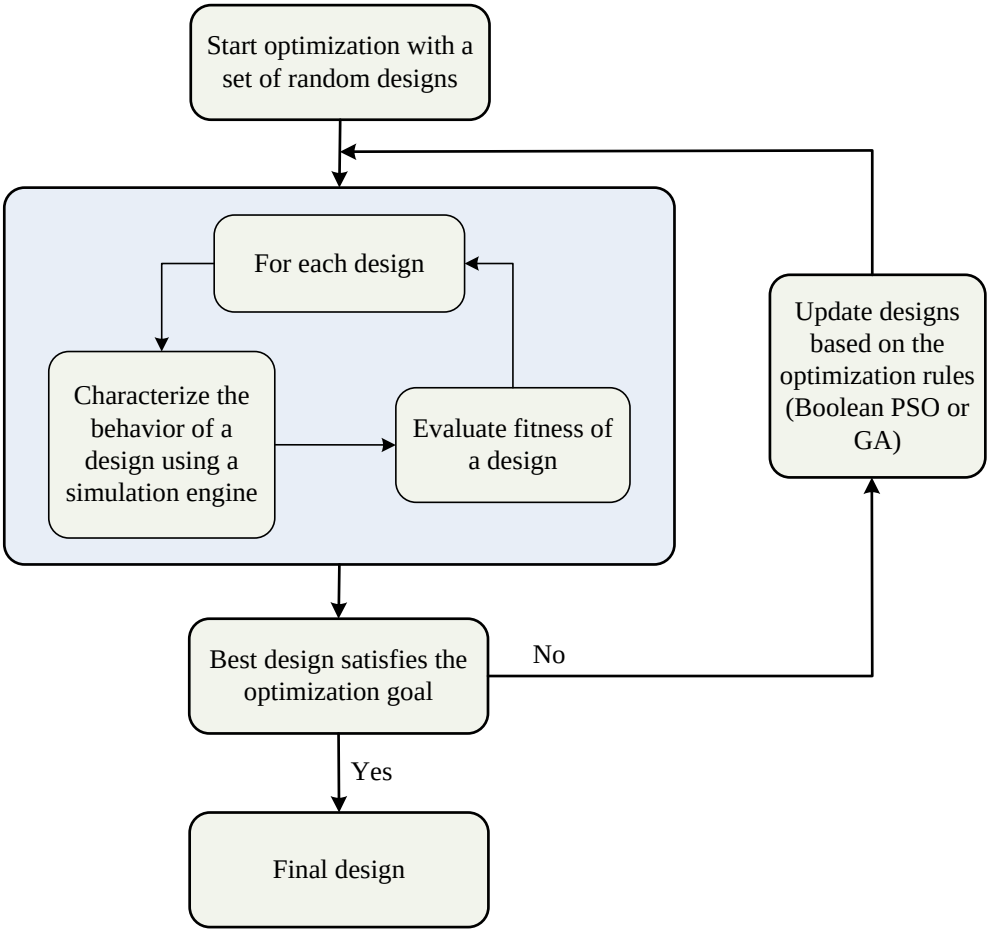

Figure 1.1: Schematic representation of an inverse design tool combining an evolutionary algorithm with a simulation engine.

Photonic Crystals

The rapid enhancement of photonic technology has led to great demand for decreasing the size of optical devices. Compact devices can be densely integrated and as a consequence, they can reduce the fabrication cost greatly. Structures with large refractive index contrast materials can confine light effectively; this is the enabling technology for building compact devices.

Photonic crystals (PCs) have been shown to be promising structures for high-density integrated optics [22]. PCs are periodic structures of high and low refractive index materials. By introducing defects (destroying the periodicity) into photonic crystal structures, light can be manipulated in a variety of ways which has resulted in various compact devices such as multiplexers and demultiplexers [23], power splitters [24], sharp waveguide bends [25], and lasers [26]. Figure 1.2 shows a microcavity in a photonic crystal waveguide designed to operate at $\lambda = 1.54$ μm [1]. It is clear that the device size is at the order of the operating wavelength.

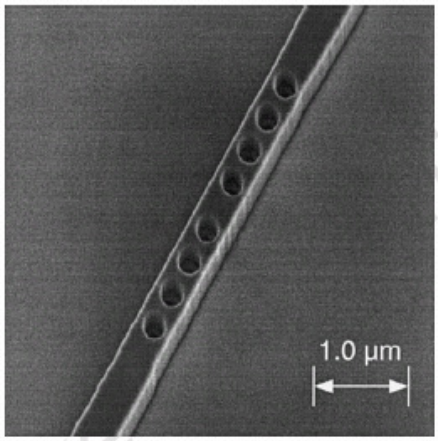

Figure 1.2: A photonic crystal waveguide microcavity. The figure is reprinted from [1].

PC devices are normally designed by intuition or by varying some design parameters such as the size and position of PC elements using trial and error guided by

intuition. However, these design approaches are limited in many ways. They depend on the level of insight into the problem at hand. To reach solutions that might not be obtained by direct design, using inverse design methods is inevitable.

Binary Supergratings

Binary supergratings (BSG) have been shown to provide almost arbitrary wavelength response [27]. BSG uses an aperiodic structure with a fixed element length and two allowed refractive index values for each element. These constraints make the BSG well-suited to semiconductor fabrication, because it only requires a single lithographic step. However, BSG structures do not provide compact devices because a weak refractive index contrast has been used in their structures so far. This is the limitation of past design techniques which are based on Fourier methods. Figure 1.3 depicts an schematic of a tunable laser in which two grating filters are used [2]. Although the rear grating provides multi-wavelength filtering from 1.52 μm to 1.60 μm, its total length is more than 1000 times the operating wavelength.

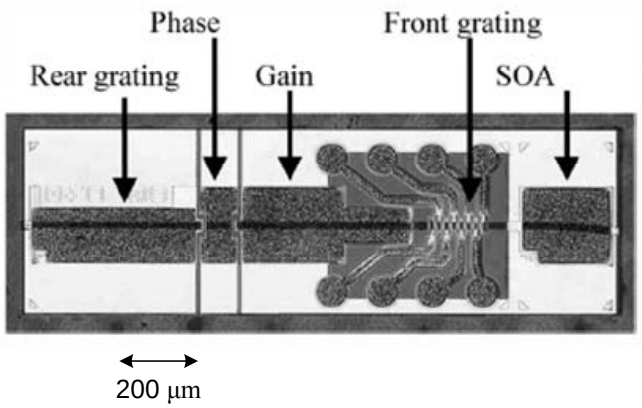

Figure 1.3: Schematic representation of a widely tunable laser. Figure is reprinted from [2].

Combining the concept of BSG with large refractive index changes may provide compact devices similar to the idea in photonic crystals. However, because BSG

design problems with high refractive index changes are highly nonlinear, previously proposed Fourier methods cannot be used to design them. Similarity between photonic crystal and binary super-grating problems and the large number of elements involved in BSGs make the Boolean PSO based inverse design an appropriate approach for designing them.

1.1 Research Objectives

The main objectives of the research presented in this thesis are two-fold:

- Development of an inverse design technique to design photonic crystals
  - Implement the scattering matrix method to simulate the behavior of photonic crystal structures
  - Combine Boolean particle swarm optimization with scattering matrix method as a new method of designing photonic crystals
  - Design a photonic crystal lens with a very low F-number by the proposed method
  - Compare Boolean PSO results with genetic algorithm results
- Development of an inverse design technique to design binary supergratings with large refractive index changes
  - Implement the transmission matrix method to simulate the behavior of binary supergratings
  - Combine Boolean particle swarm optimization with transmission matrix method as a new method of designing BSGs
  - Validate the method

- Design compact BSG filters for applications such as tunable lasers and intrachip optical networks
- Compare Boolean PSO results with genetic algorithm results

1.2 Thesis Contribution

A new inverse design method for designing two-dimensional photonic crystals is proposed. This method combines scattering matrix method as the simulation tool with Boolean PSO as the optimizer. A photonic crystal lens with a very low F-number is designed by this method which can be used as an interface between a photonic crystal waveguide and a conventional single-mode fiber.

Furthermore, the concept of binary supergrating with large refractive index changes is presented for the first time. This allows for compact devices with arbitrary wavelength response while benefiting from a single-step lithography process. A combination of Boolean PSO and transmission matrix method is presented as a new inverse design method for binary supergratings. Two problems with limited dimensions are used to validate the proposed method. Pass-band filters for wavelength-division multiplexing, wavelength-selective filters, a broadband filter for intrachip optical netwroks, and a multi-wavelength filter for tunable lasers are designed by this method.

1.3 Thesis Outline

Chapter 2 consists of a review of particle swarm optimization, its conventional binary version, Boolean particle swarm optimization and genetic algorithm.

A review of two-dimensional photonic crystals and previous inverse design techniques for PC structures are briefly reviewed in chapter 3. Then, our proposed method

of designing PCs is described followed by a review of scattering matrix method. The results of designing a PC lens by using this method is presented after that. Replacing Boolean PSO with genetic algorithm in the lens design problem, a comparison between these two methods is provided.

Binary supergrating with large refractive index changes is described in chapter 4. The proposed inverse design method and the transmission matrix method are explained. Then two examples consisting of a cavity sandwiched between two Bragg reflectors and a BSG with a random refractive index distribution used to validate the method are described. The results of using this method to design filters for four different applications are presented. The results are compared to genetic algorithm in some cases.

Conclusions and suggestions for further work are given in chapter 5.

Chapter 2

Boolean Particle Swarm Optimization

2.1 Introduction

Particle swarm optimization (PSO) is a powerful evolutionary algorithm for solving single or multi-objective optimization problems with real-valued or discrete parameters [28]. PSO is simple in concept, few in parameters, and easy in implementation, besides it has an excellent optimization performance. At first, PSO was introduced for continuous search spaces and because of the aforementioned features, it has been widely applied to many optimization problems soon after its introduction. However, the original binary version of PSO attracted much lesser attention because it is not as efficient as the original PSO [29].

Boolean PSO is a novel representation of PSO algorithm for binary spaces which is introduced based on the idea of using the Boolean algebra in the implementation of PSO concepts. It has been shown that Boolean PSO is a promising algorithm in dealing with various engineering design problems such as antenna design [30, 20], grating design [31, 32], design of multi-frequency dividers [33], and design of photonic crystal structures [34]. The better optimization performance of Boolean PSO in comparison with genetic algorithm (GA) in some design cases has been also demonstrated [21, 20].

This chapter starts with an overview of PSO. The conventional binary PSO is then studied to show why it is not as efficient as the original PSO. After that, the Boolean PSO is presented. In this thesis, the Boolean PSO results are compared with GA results in many cases. Therefore, genetic algorithm is briefly reviewed in the final section.

2.2 Particle Swarm Optimization

Particle swarm optimization is a stochastic search algorithm developed by Eberhart and Kennedy, an electrical engineer and a psychologist, in 1995 [13]. This algorithm simulates the behavior of a social system such as a swarm of bees or a flock of birds looking for a place with the highest amount of flowers or food in a field.

To explain how PSO algorithm works, an optimization problem which requires optimization of N variables simultaneously is considered here. PSO is initialized with a population of solutions, called "particles". At first, a random position and velocity is assigned to each particle. The position of each particle corresponds to a possible solution for the optimization problem. A fitness number is assigned to each particle which shows how good its position is. During the optimization process, each particle moves through the N-dimensional search space with a velocity that is dynamically adjusted according to its own and its companion's previous behavior. Updating the particle velocity is based on three terms, namely the "social," the "cognitive," and the "inertia" terms. The "social" part is the term guiding the particle to the best position achieved by the whole swarm of particles so far (g_{best}), the "cognitive" part guides it to the best position achieved by itself so far (p_{best}), and the "inertia" part is the memory of its previous velocity ($\omega.v_n$). The following formulae demonstrate the updating process of a particle position (x_n) and its velocity (v_n) in the n^{th} dimension in an N-dimensional optimization space:

$$v_{n+1} = \omega \,.\, v_n \,+\, c_1 \,.\, \phi_1 \,.\, (p_{best,n} - x_n) \,+\, c_2 \,.\, \phi_2 \,.\, (g_{best,n} - x_n) \tag{2.1}$$

$$x_{n+1} = x_n \,+\, v_{n+1} \tag{2.2}$$

In equation 2.1, ϕ_1 and ϕ_2 are random numbers uniformly distributed between 0 and 1. c_1 and c_2 are acceleration constants and ω is the inertia weight. These three parameters determine the tendency of the particles to the related terms. Moreover, another parameter is used to limit the maximum velocity of a particle (V_{max}). All these parameters directly affect the optimization behavior; for example, the inertia weight controls the exploration ability of the process while the acceleration constants and maximum velocity are parameters for controlling the convergence rate [35, 36].

The iterative procedure of updating the velocities and positions of particles continues until the best position achieved by the whole swarm of particles (g_{best}) does not change over several iteration. A flowchart describing the PSO algorithm is shown in Figure 2.1.

2.3 Conventional Binary Particle Swarm Optimization

Although PSO has attracted much attention for real-valued optimization problems, there have been few attempts to apply the idea to the discrete and especially binary optimization ones [28]. In a binary PSO, the position of each particle is represented by a binary string. The first binary PSO introduced by Kennedy and Eberhart [37] uses the same terms as in the original PSO, but the velocity of a particle is defined as the probability that a particle might change its state to 1. Unlike real-valued PSO, this algorithm is not used widely and there have been several attempts to hybridize it with other algorithms to achieve better performance [38]. Moreover, this method

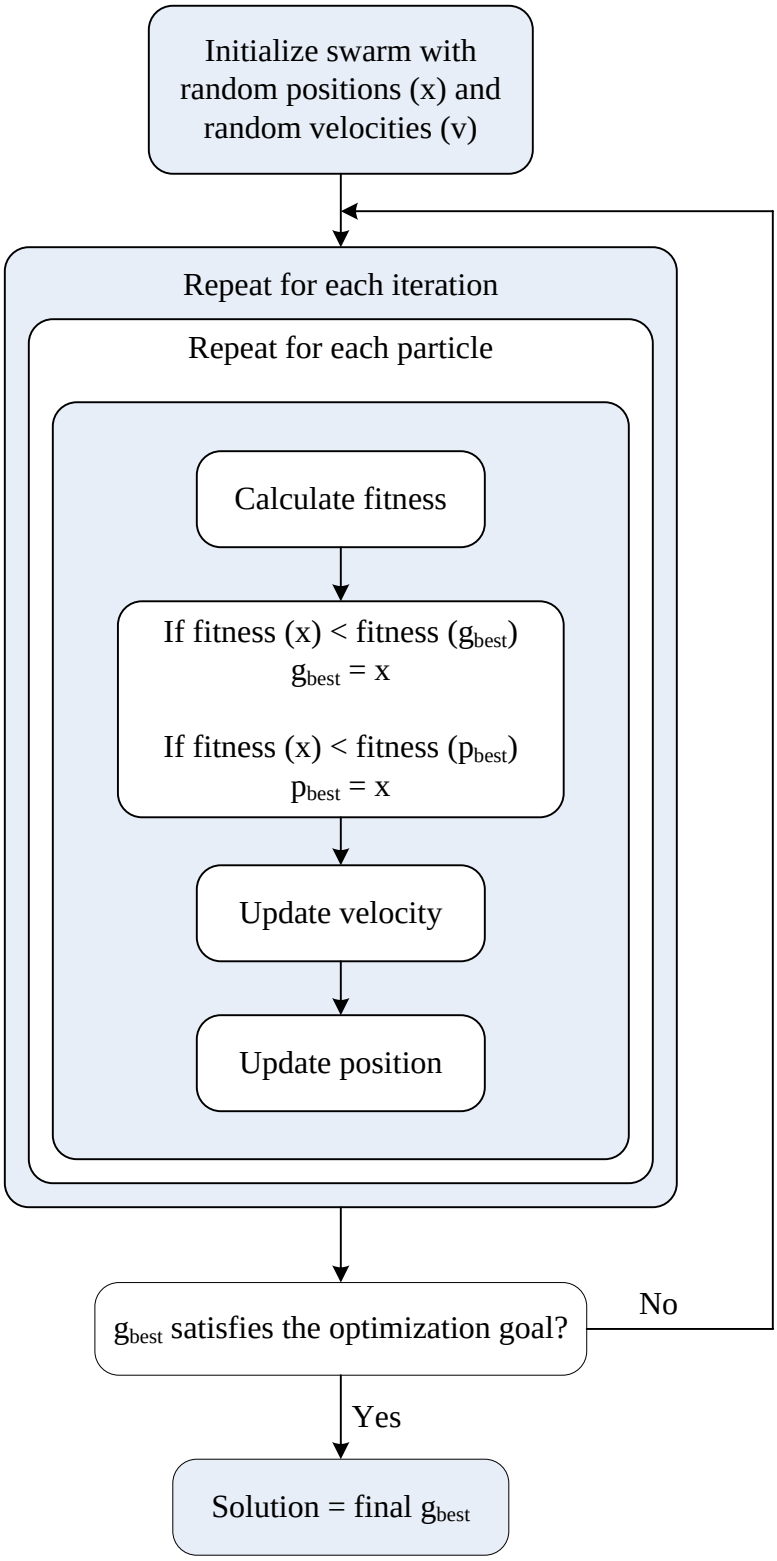

Figure 2.1: Flowchart depicting the PSO algorithm.

does not seem to outperform the commonly used binary optimization methods such as genetic algorithms [21].

In this binary PSO, the idea of using "probability of being 1 in the binary space" instead of "velocity" has resulted in the following equations for updating each bit of a particle [37]:

$$v_{d+1} = v_d \; + \; \phi_1 \,.\, (p_{best,d} - x_d) \; + \; \phi_2 \,.\, (g_{best,d} - x_d) \tag{2.3}$$

$$S(v_{d+1}) = \frac{1}{1 \; + \; e^{-v_{d+1}}} \tag{2.4}$$

$$\text{if} \quad (rand\,() \; < \; S(v_{d+1})) \quad \text{then} \quad x_{d+1} \; = \; 1; \qquad \text{else} \quad x_{d+1} = 0 \tag{2.5}$$

v_d is the probability of the d$^{\text{th}}$ bit of a particle to become 1 while Equation 2.3 represents its dependence on the previous value of v_d, best positions achieved by all the particles (g_{best}) and by the particle in question (p_{best}) so far. Because the calculated v_d can be greater than 1 or less than 0, a sigmoid function (Equation 2.4) is used to transform this value into the limits such that it can be used as a probability. A random generator over $[0, 1]$, $rand()$, is used to specify the state of each bit (Equation 2.5). ϕ_1 and ϕ_2 are random numbers uniformly distributed between 0 and 1. The parameter V_{max} in this algorithm is retained, but unlike real-valued PSO, small values for V_{max} promotes exploration.

By checking all the states of x_d, p_{best}, and g_{best} it can be seen that the conventional binary PSO generally can track the main idea of the PSO, which is the tendency of particles to approach their previous best position and global best position; however, it

has some considerable disadvantages because the considered velocity and distance are not of the same nature. Showing the adverse effects of this idea on the performance of the algorithm needs a detailed study of the method and comparison between the concepts of the binary and real algorithms, which is not aimed in this thesis. However, a special case focusing on the inertia weight is examined here to seek to know why this method has not become popular like the algorithm for real-valued problems.

In this binary PSO, the concept of inertia weight is very different from real-valued PSO. In fact, the effect of this parameter is opposite of that for real-valued PSO. The inertia is the tendency of each particle to keep its previous movement, the change of the bit in a binary space. However, in this method this tendency cannot be inferred from the first term of Equation 2.3. Not only is there no coefficient to perform the task of the inertia weight, which specifies the rate of this tendency, but also this term shows the tendency of the bit to become one. For example, consider a large value of v_d which results in $S(v_d) \approx 1$, so x_d with a high probability will become 1 in the next step. If the p_{best} and g_{best} have not changed in the current step, the new $\mathrm{v_d}$ will be unchanged; therefore, the new v_d dictates x_d to still remain at 1. However, this behavior cannot fulfill the desired function of the inertia.

In addition, as a consequence of using Equation 2.4, the concept of the maximum velocity V_{max} is not valid. In summary, the above discrepancies have deteriorated the conventional binary PSO versus the real-valued PSO.

2.4 Boolean Particle Swarm Optimization

The Boolean particle swarm optimization is a new evolutionary algorithm implemented by means of the Boolean algebra to meet the requirements of a real-valued particle swarm optimization [20, 21]. It is shown to outperform the conventional binary PSO and GA in some well-known test functions such as De Jong's, Rastrigin's

and Griewangk's functions [21]. It has been also shown that Boolean PSO is effective in dealing with various electromagnetic problems, such as antenna design [20, 30], grating design [31], and design of photonic crystal structures [34].

In the Boolean PSO, distance and velocity are defined based on the difference between corresponding bits of two binary strings. The "and" (.), "or" (+), and "xor" ($\oplus$) operators are used to model movement of the particles. Main formulae for updating the d^{th} bit of position and velocity of each particle are:

$$v_{d+1} = \omega \,.\, v_d \;+\; c_1 \,.\, (p_{best,d} \oplus x_d) \;+\; c_2 \,.\, (g_{best,d} \oplus x_d) \tag{2.6}$$

$$x_{d+1} = x_d \oplus v_d \tag{2.7}$$

The distance between two bits is another bit whose value represents their difference. Consequently, the velocity bit, v_d, determines whether the d^{th} bit of the position of the particle, x_d, should change in the next step, according to Equation 2.7. In Equation 2.6, the second and third terms calculate the distance between (x_d, $p_{best,d}$) and (x_d, $g_{best,d}$), respectively. The three terms are then combined using "or" operators. c_1, c_2 as the acceleration coefficients and ω as the inertia coefficient are binary bits stochastically set from the system parameters C_1, C_2, Ω, acceleration constants and inertia weight, which are real numbers between 0 and 1. The probabilities for being "1" of c_1, c_2, ω are C_1, C_2, and Ω. The procedure used to specify the velocity for each bit of a particle is depicted in the schematic diagram of Figure 2.2. In this procedure, V_{max} is the number of allowed "1" bits in the calculated velocity array. To prevent the particles from moving faster than this value, each calculated velocity array is examined for the number of "1". If this number exceeds the desired value, one bit with a value of "1" is set to zero randomly, and this process continues

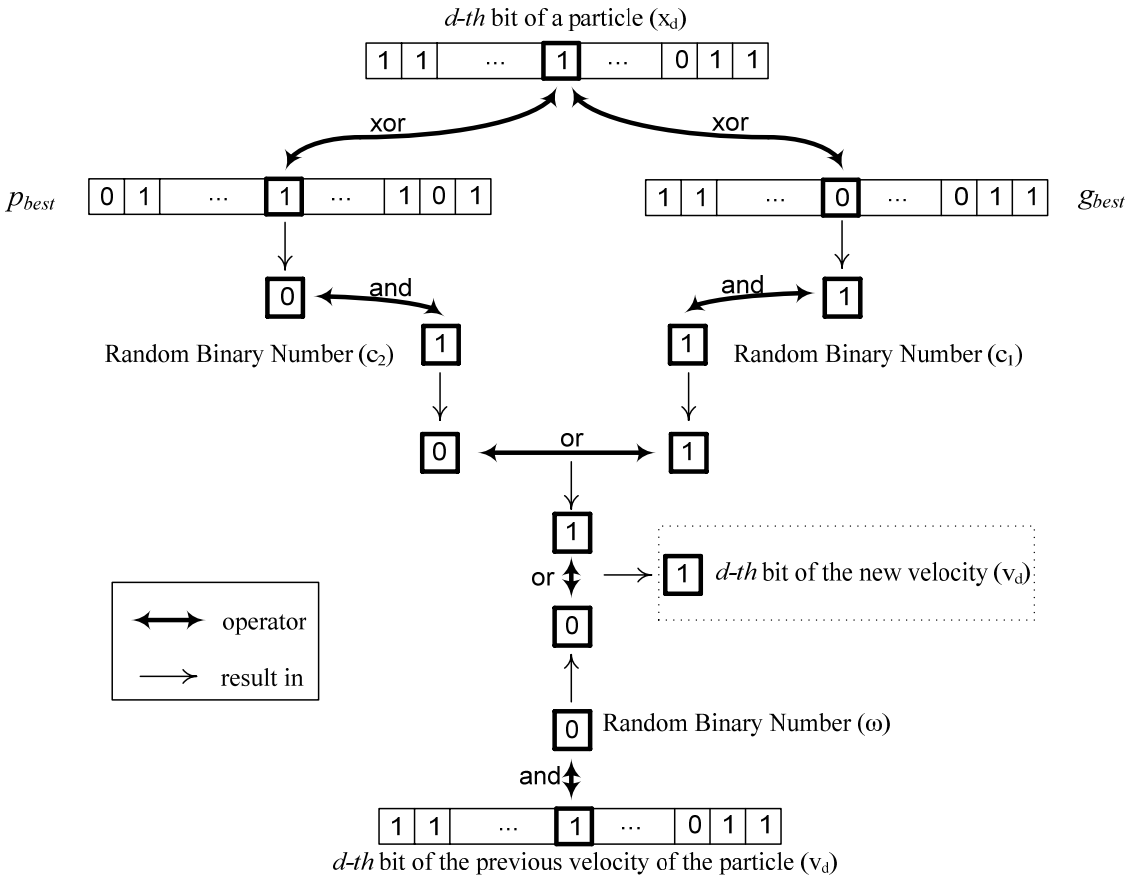

Figure 2.2: Process of updating the velocity in the Boolean PSO.

until the satisfaction of the criterion.

The simplicity in the implementation of Boolean PSO and also the straightforward influence of its parameters on the optimization process are its key benefits over the conventional binary PSO and also the genetic algorithm. Its superior performance over those methods in some cases has been shown in [21].

2.5 Genetic Algorithm

Genetic algorithm (GA) is a very popular class of evolutionary algorithms introduced in the early 70s by Holland [39]. The concept of "survival of the fittest" from Darwin's

theory of evolution combined with simulated genetic operators from nature form the basis for GA. GA optimization starts with a population of N random solutions called "chromosomes". Each chromosome is a binary string. A fitness value is assigned to each chromosome which shows that how fit the chromosome is.

GA updates the chromosomes using three main operators: "selection", "crossover", and "mutation". "Selection" operator chooses chromosomes for reproduction process so that a chromosome with a better fitness has a better chance of being selected. A number of selection strategies have been developed for GA optimization [40]. Two of the most widely used selection strategies are roulette-wheel selection and tournament selection. In roulette-wheel selection, chromosomes are selected based on a probability of selection given in Equation 2.8, where $f(chromosome_i)$ is the fitness of the i$^{\text{th}}$ chromosome:

$$P_{selection} = \frac{f(chromosome_i)}{\sum_{i=1}^{N} f(chromosome_i)} \tag{2.8}$$

Therefore, the probability of selecting a chromosome from the population is a function of the relative fitness of the chromosome. In tournament selection, a sub population of M chromosomes is chosen at random from the population. The chromosomes of this sub-population compete in the basis of their fitness. The chromosome in the sub-population with the highest fitness becomes the selected chromosome. All of the sub-population members are then placed back into the general population and the process is repeated.

Once two chromosomes have been selected as parents through the "selection operator", two children are created by recombining and mutating the chromosomes of the parents. The "crossover" operator combines two parents and generates two children based on the *crossover rate*. The *crossover rate* is the probability of swapping bits

between two chromosomes. Many variations of crossover have been developed. The simplest form is single-point crossover. The single-point crossover chooses a random point along the chromosomes and then exchange all the the bits after that point as depicted in Figure 2.3.

Before the generated chromosomes are transfered to the next iteration, the "mutation" operator flip some of their bits based on the *mutation rate*. The *mutation rate* is the probability of flipping a bit within the chromosome. Mutation of chromosomes results in exploring new areas of the search space.

Many extensions have been applied to the simple GA optimizer described above to improve its performance. One of the most important extensions is the elitist strategy [40]. In the original GA, it is possible for the next iteration to have a best chromosome with a worse fitness than a preceding iteration. To overcome this problem, a simple test has been added to GA to verify that the best chromosome in the new iteration is at least as good as the one from the preceding iteration. A certain number of best chromosomes from one iteration are guaranteed to survive to the next iteration. Elitism is used to ensure that there is a continuous improvement in the best fitness of the population as a function of time.

Using three main operators of selection, crossover, and mutation and applying the elitist strategy, the procedure of updating the chromosomes continues until a new population with N chromosomes are generated. If the fittest chromosome does not change over several iterations, the optimization is terminated. A flowchart describing the basic GA algorithm is shown in Figure 2.3.

2.6 Conclusion

In this chapter, particle swarm optimization and its conventional binary version were reviewed. Boolean PSO, which is a PSO algorithm implemented by means of the

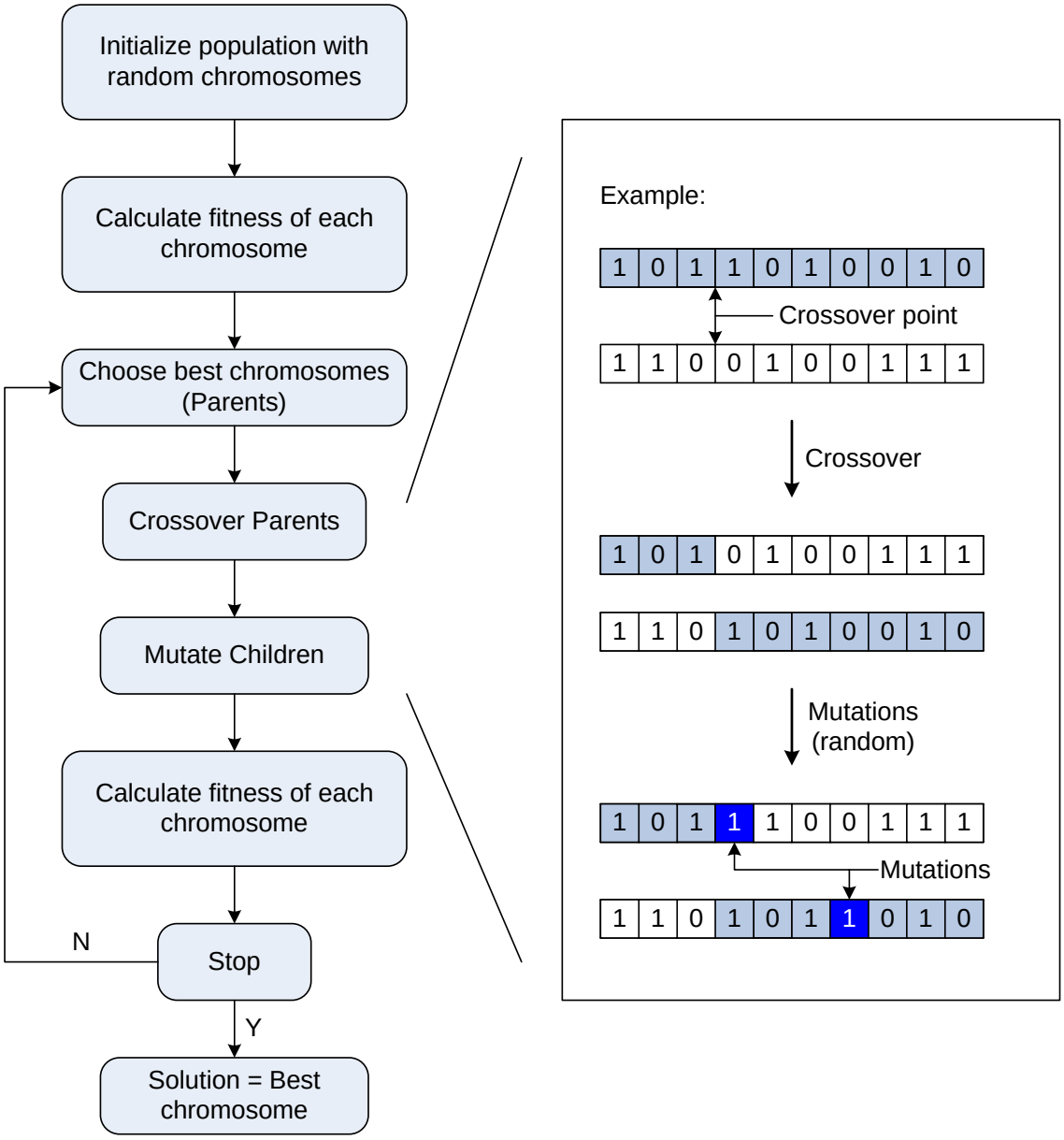

Figure 2.3: Flowchart depicting the GA algorithm. Breakout: An example illustrating the crossover and mutation operators.

Boolean algebra for use in binary optimization problems, was also studied. In Boolean PSO, the behavior of particles according to three PSO terms, i.e., "social," "cognitive," and "inertia" was discussed and compared with the conventional PSO. In this thesis, Boolean PSO results are compared to genetic algorithm results in many cases. Thus, GA was briefly reviewed in the last section. In comparison with GA, PSO has only one simple operator, which is "velocity updating". Moreover, control parameters have simpler definition in PSO. Although in many cases both algorithms result in good solutions, the simpler implementation and reduced bookkeeping of PSO make it appealing [41].

Chapter 3

Design of Photonic Crystal Structures

3.1 Introduction

Photonic crystals (PCs) are periodic dielectric structures which are designed to manipulate and control the flow of light. The periodic refractive index variation in PC structures results in frequency bands and frequency gaps (bandgaps) for photons. The photonic crystal does not allow any propagation of photons with frequencies falling in the bandgap, while allowing other frequencies to propagate freely. The two-dimensional PC is the most common type of PC since it is easier to fabricate and particularly useful in integrated optics. Two-dimensional PCs are often made by etching air holes into a planar dielectric slab as depicted in Figure 3.1.

In this chapter, we propose a new inverse design method for designing two-dimensional PC structures. The method combines Boolean PSO as the optimization technique with Scattering Matrix Method as the simulation tool. The potential of this approach is illustrated in a lens design problem. The appropriate behavior of the optimization process in comparison with genetic algorithm is also presented.

This chapter starts with a brief review of properties of two-dimensional PCs and the previous methods of designing them. Then, the proposed method of designing

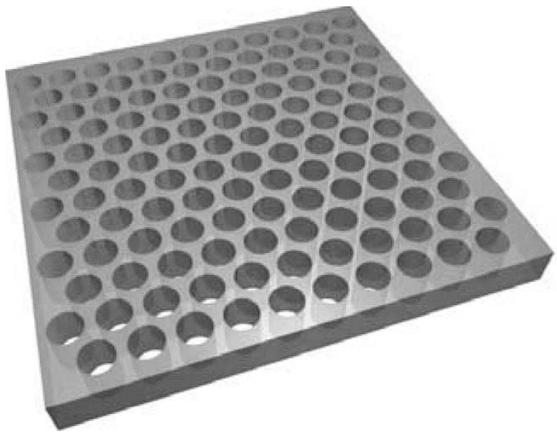

Figure 3.1: Schematic representation of a two-dimensional photonic crystal consisting of a hexagonal lattice of air holes patterned in a slab of dielectric. Figure is reprinted from [3].

two-dimensional PCs is described. Finally, the lens design problem and the results are presented.

3.2 Background

The properties of two-dimensional PCs are determined by two main factors: the refractive index contrast between the slab and the material filling the holes, and the arrangement of holes in the lattice [42]. Considering the former factor, a high refractive index contrast results in a large bandgap for the PC. As to lattice configuration, it is often altered by introducing defects (removing holes) into the lattice. For example, a row of holes can be removed from a two-dimensional PC structure to form a waveguide as depicted in Figure 3.2 (a). This structure only allows light transmission along the line defect for frequencies in the bandgap of the surrounding PC. As another example, by removing a few holes or creating a point defect, an optical resonator can be formed as shown in Figure 3.2 (b).

Altering lattice configuration in PC structures is not limited to only incorporating point or line defects. By using inverse design techniques, the functionality of many

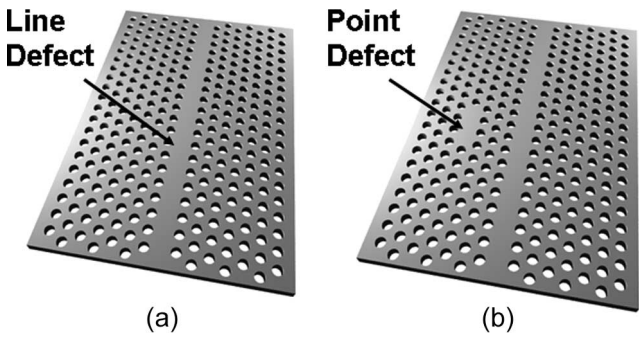

Figure 3.2: Schematic representations of (a) a line defect (b) a point defect in a hexagonal PC lattice. Figure is reprinted from [4].

known PC devices has been enhanced or new structures have been proposed. For example, the diameter and distance between the holes can be optimized to obtain an ultra-flattened dispersion holey fiber [5], as illustrated in Figure 3.3. As another example, in a Z-bend waveguide depicted in Figure 3.4, the shape of the holes around the bend can be optimized to obtain low loss transmission over a wide bandwidth [6].

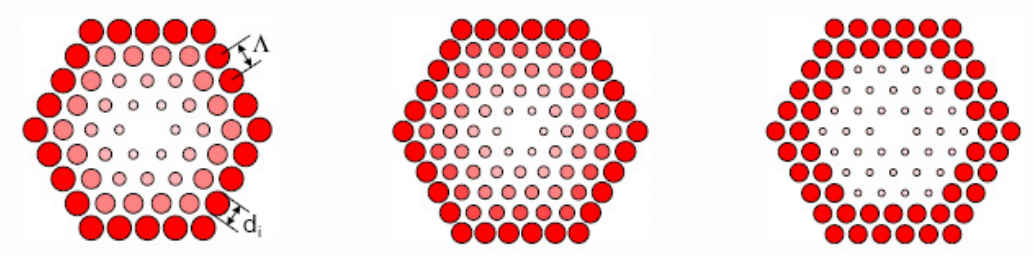

Figure 3.3: Holey fibers optimized by an inverse design technique for maximum flattened dispersion. Figure is reprinted from [5].

In these examples, the starting design is known but it is not quite satisfactory and the optimization gradually modify it to improve its performance. By contrast, there are other inverse design problems that only the general form of the PC structure, some constraints, and the desired functionality is known, but the optimization process generates its own starting designs. Figure 3.5 depicts a 1×2 demultiplex coupler which separates and couples two wavelengths from one dielectric waveguide to two

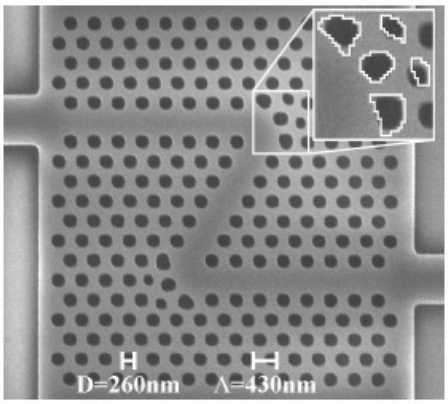

Figure 3.4: The optimized Z-bend. The number, size, and shape of the holes at each bend is optimized. The operating frequency of the Z-bend is within the bandgap of the surrounding PC. Figure is reprinted from [6].

separate photonic crystal waveguides [7]. The black circles are removed from the initial PC structure during the inverse design procedure.

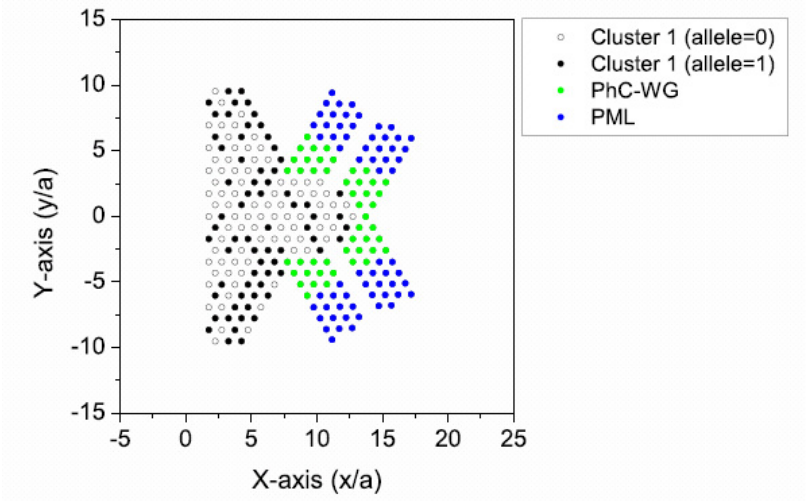

Figure 3.5: The structure of the 1 × 2 demultiplex coupler. The green circles show the photonic crystal waveguide. The blue circles absorb the waves for semi-infinite waveguide simulation. The black circles are removed from the lattice during the optimization procedure. The white circles represents the optimized structure. Figure is reprinted from [7].

3.3 Design Method

In this chapter, we focus on inverse design problems similar to the case of demultiplex coupler. We consider a dielectric slab with a hexagonal lattice of cylinders as the initial PC configuration as illustrated in Figure 3.9. This initial PC configuration is modeled with a binary string where a "1" bit means presence of a cylinder and a "0" bit means the absence of a cylinder. This binary representation of the structure makes the Boolean PSO an appropriate optimization technique for this problem.

The PC is illuminated with an incident wave and Scattering Matrix Method (SMM) is employed to simulate the wave diffraction [8]. SMM is a semi-analytical method which has various advantages over popular PC simulation methods such as finite-difference time-domain (FDTD). Considering the circular cross section of cylinders, SMM represents the incident and scattered waves in terms of Bessel functions which are natural modes for circular shapes. As a consequence, calculating the fields is simplified to calculating the coefficients of these Bessel functions which results in a very short simulation time for a limited number of cylinders.

Here, the combination of Boolean PSO and SMM is proposed to facilitate designing the optimal configuration of two-dimensional PC-based devices. A PC lens with flat surfaces which can be used as an interface to couple light from a conventional fiber to a photonic crystal waveguide is designed to validate this inverse design technique.

3.3.1 Scattering Matrix Method

The Scattering Matrix Method is an efficient method to deal with the problem of scattering by a finite number of objects having arbitrary shapes or different electromagnetic parameters [8, 43, 44, 45]. Here, the case of two-dimensional photonic

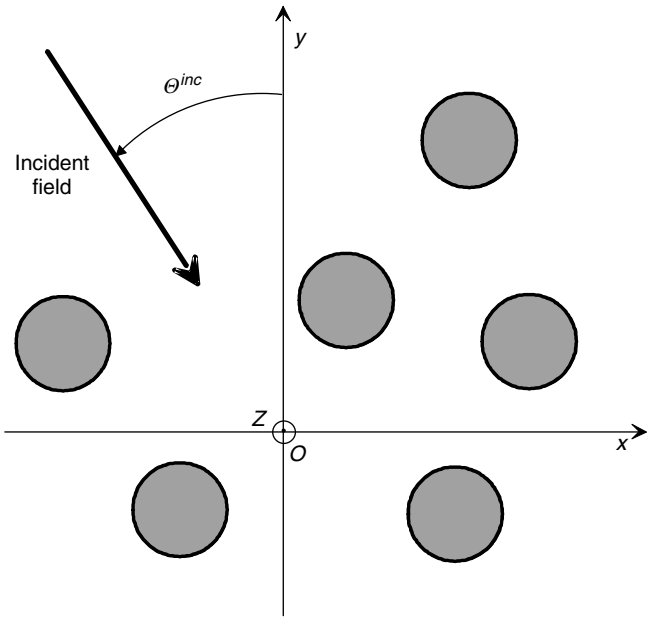

Figure 3.6: An s-polarized incident plane wave illuminates N cylinders. Figure is reprinted from [8].

crystals is considered where a set of identical cylinders of radius R and relative permittivity $\varepsilon_{r,int}$ are lying on a background material with relative permittivity $\varepsilon_{r,ext}$ as depicted in Figure 3.6. The refractive indexes of the materials inside and outside the cylinders are $n_{int} = \sqrt{\varepsilon_{r,int}}$ and $n_{ext} = \sqrt{\varepsilon_{r,ext}}$, respectively. It is assumed that the electric field of the incident plane wave is parallel to the cylinder axes (an s-polarized wave), its incidence angle and time dependence are Θ^{inc} and $exp(-i\omega t)$, respectively.

The electric field of the incident wave is assumed to be

$$\mathbf{E^i} = E_z^i \hat{\mathbf{z}} \tag{3.1}$$

with:

$$E_z^i = \exp(ik_0 n_{ext}(x \sin\Theta^{inc} - y \cos\Theta^{inc})) \tag{3.2}$$

Maxwell's equations result in the total electric field satisfying the following Helmholtz equation at any point of space:

$$\nabla^2 E_z + k_0^2 \varepsilon_r(x, y) E_z = 0 \tag{3.3}$$

where E_z and its normal derivative must be continuous at the boundaries.

SMM consists of the following three main steps when dealing with a scattering problem including the above example:

1- It is shown that the total field can be written as Fourier-Bessel series. The series consists of two parts outside a cylinder: one part is the total incident field on the cylinder and other part is the field which is scattered by the cylinder. The total incident field includes the incident plane wave in addition to the field scattered by other cylinders in the direction of the considered cylinder.

2- The causality relation between the total incident field on a cylinder and the field scattered by that cylinder is written in the form of Fourier-Bessel coefficients.

3- In this step, the coupling between all cylinders is considered by writing the total incident field on a cylinder as the sum of the incident plane wave and the field scattered by other cylinders.

Applying above steps for a scattering problem simplifies the determination of the field distribution to the evaluation of a set of complex coefficients.

Representing the Fields Inside and Outside the Cylinders by Fourier-Bessel Series

Here, we assume a local polar coordinate system (r_j, θ_j) with an origin at the center of each cylinder (O_j) as depicted in Figure 3.7.

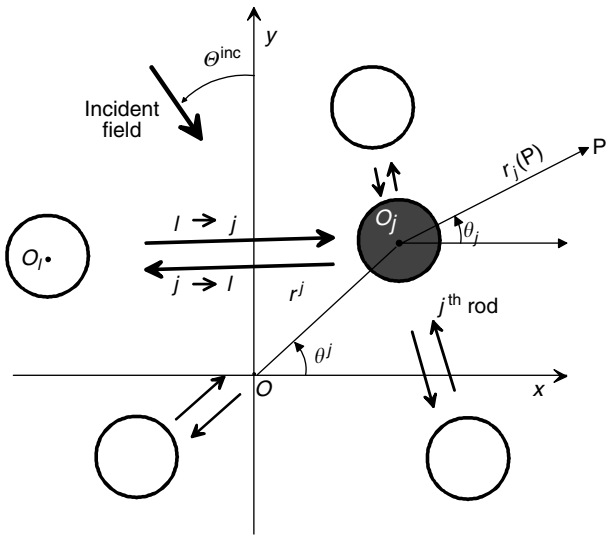

Figure 3.7: The local coordinate system associated with the j^{th} cylinder. $j \rightarrow l$ shows the field scattered by the j^{th} cylinder toward the l^{th} cylinder. Figure is reprinted from [8].

At point P the total electric field can be expressed as:

$$E_z(r_j, \theta_j) = \sum_{m \in Z} E_{z,m}(r_j) \exp(im\theta_j) \tag{3.4}$$

If P is inside the cylinder, the total electric field satisfies the following Helmholtz equation:

$$\nabla^2 E_z + k_0^2 \varepsilon_{r,int} E_z = 0 \tag{3.5}$$

By substituting the expression of the field in Equation 3.4 into Equation 3.5 and expanding the field in terms of Fourier-Bessel series, it is shown that the total field inside a cylinder can be expressed as:

$$\text{if} \quad \mathrm{r_j} < \mathrm{R} : \qquad E_z(r_j, \theta_j) = \sum_{m \in Z} c_{j,m} J_m(k_0 n_{int} r_j) \exp(im\theta_j) \tag{3.6}$$

where J_m is the Bessel function of the $\mathrm{m^{th}}$ order and of the first kind. Thus, by evaluating the coefficients $c_{j,m}$ in Equation 3.6, the total field inside the cylinder is

determined.

If P is outside the cylinder, the total electric field can be expressed in terms of Fourier-Bessel series as:

if $\mathrm{r_j} > \mathrm{R}$:

$$E_z(r_j, \theta_j) = \sum_{m \in Z} a_{j,m} J_m(k_0 n_{ext} r_j) \exp(im\theta_j) + \sum_{m \in Z} b_{j,m} H_m^{(1)}(k_0 n_{ext} r_j) \exp(im\theta_j) \tag{3.7}$$

where $H_m^{(1)}$ is the Hankel function of the $\mathrm{m^{th}}$ order and is defined as:

$$H_m^{(1)}(u) = J_m(u) + iY_m(u) \tag{3.8}$$

Y_m is the Bessel function of the $\mathrm{m^{th}}$ order and of the second kind.

Causality Relation for Each Cylinder

In Equation 3.7, the first part represents the total incident field on $\mathrm{j^{th}}$ cylinder which consists of the incident plane wave and the field scattered by other cylinders in the direction of the $\mathrm{j^{th}}$ cylinder. The second part shows the field scattered by the $\mathrm{j^{th}}$ cylinder. There is a causality relation between these two parts:

$$\mathbf{b_j} = \mathbf{S_j a_j} \tag{3.9}$$

where $\mathbf{S}_\mathrm{j}$ is an infinite-dimension square matrix.

The electric field and its normal derivative must be continuous across the boundary of each cylinder; using the field expansions given in Equations 3.6 and 3.7 at the boundary of a cylinder ($r_j = R$) results in:

$$a_{j,m}J_m(k_0 n_{ext}R) + b_{j,m}H_m^{(1)}(k_0 n_{ext}R) = c_{j,m}J_m(k_0 n_{int}R) \tag{3.10}$$

$$a_{j,m}\left.\frac{d(J_m(k_0 n_{ext}r_j))}{dr_j}\right|_{r_j=R} + b_{j,m}\left.\frac{d(H_m^{(1)}(k_0 n_{ext}r_j))}{dr_j}\right|_{r_j=R} = c_{j,m}\left.\frac{d(J_m(k_0 n_{int}r_j))}{dr_j}\right|_{r_j=R} \tag{3.11}$$

By eliminating $c_{j,m}$ between Equations 3.10 and 3.11, the following relation between $b_{j,m}$ and $a_{j,m}$ can be obtained:

$$b_{j,m} = -\frac{J_m(k_0 n_{ext}R)\left.\frac{d(J_m(k_0 n_{int}r_j))}{dr_j}\right|_{r_j=R} - J_m(k_0 n_{int}R)\left.\frac{d(J_m(k_0 n_{ext}r_j))}{dr_j}\right|_{r_j=R}}{H_m^{(1)}(k_0 n_{ext}R)\left.\frac{d(J_m(k_0 n_{int}r_j))}{dr_j}\right|_{r_j=R} - J_m(k_0 n_{int}R)\left.\frac{d(H_m^{(1)}(k_0 n_{ext}r_j))}{dr_j}\right|_{r_j=R}}\, a_{j,m} \tag{3.12}$$

Equation 3.12 shows that the $\mathbf{S}_\mathrm{j}$ matrix is diagonal and it is defined by:

$$S_{m,m} = -\frac{J_m(k_0 n_{ext}R)\left.\frac{d(J_m(k_0 n_{int}r_j))}{dr_j}\right|_{r_j=R} - J_m(k_0 n_{int}R)\left.\frac{d(J_m(k_0 n_{ext}r_j))}{dr_j}\right|_{r_j=R}}{H_m^{(1)}(k_0 n_{ext}R)\left.\frac{d(J_m(k_0 n_{int}r_j))}{dr_j}\right|_{r_j=R} - J_m(k_0 n_{int}R)\left.\frac{d(H_m^{(1)}(k_0 n_{ext}r_j))}{dr_j}\right|_{r_j=R}} \tag{3.13}$$

and

$$S_{m,n} = 0 \quad \text{if} \quad n \neq m \tag{3.14}$$

Because the cylinders are identical, their $\mathbf{S}_\mathrm{j}$ matrices are also identical. Thus, we define $\mathbf{S}_\mathrm{j} = \mathbf{S}$ for all the cylinders.

The Coupling Between the Cylinders

By considering the coupling between the cylinders, another relationship between **a** and **b** matrices can be obtained. One component of the total incident field on a cylinder is composed of the field scattered by other cylinders toward this cylinder. However, the incident field on a cylinder is defined in its local coordinate system, while the scattered fields by other cylinders are defined in the local coordinate systems associated with those cylinders. To overcome this problem, all fields are represented in a unique coordinate system associated with the j$^{\text{th}}$ cylinder. By using Graf's formula [46] and the notation of Figure 3.8, these fields can be related as:

$$H_m^{(1)}(k_0 n_{ext} r_l(P)) \exp(im\theta_l(P)) = \sum_{q \in Z} \exp(i(m-q)\theta_j^l) H_{q-m}^{(1)}(k_0 n_{ext} r_j^l) J_q(k_0 n_{ext} r_j(P)) \exp(iq\theta_j(P)) \tag{3.15}$$

Using Equations 3.7 and 3.15, it can be shown that the following matrix equation represents the relationship between the total incident field on the j$^{\text{th}}$ cylinder ($\mathbf{a}_{\text{j}}$), and the fields scattered by other cylinders toward this cylinder ($\mathbf{b}_{\text{l}}$):

$$\mathbf{a}_{\text{j}} = \mathbf{Q}_{\text{j}} + \sum_{\text{l} \neq \text{j}} \mathbf{T}_{\text{j,l}}\, \mathbf{b}_{\text{l}} \tag{3.16}$$

where $\mathbf{Q}_{\text{j}}$ is a column matrix and its elements are defined by:

$$Q_{j,m} = (-1)^m \exp(ik_0 n_{ext} r^j \sin(\Theta^{inc} - \theta^j) - im\Theta^{inc}) \tag{3.17}$$

and $\mathbf{T}_{\text{j,l}}$ is a square matrix given by:

$$T_{j,l,m,q} = \exp(i(q-m)\theta_j^l) H_{m-q}^{(1)}(k_0 n_{ext} r_j^l) \tag{3.18}$$

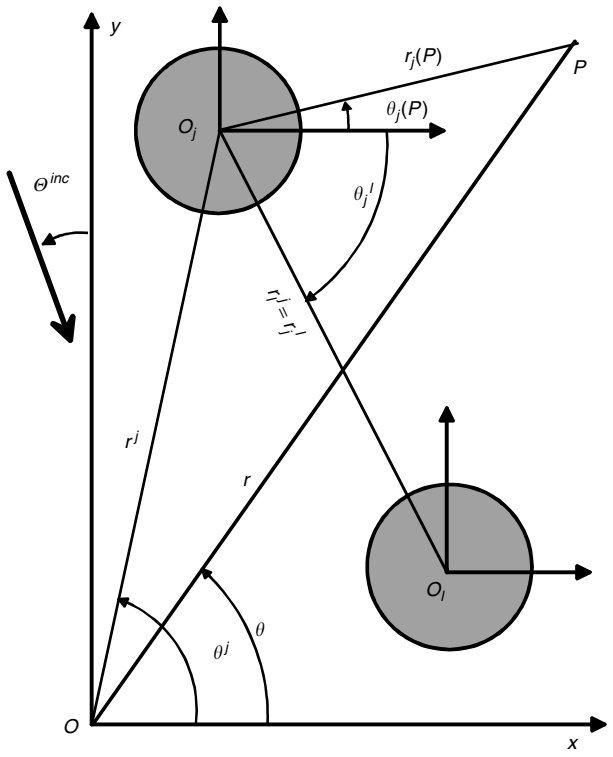

Figure 3.8: The coordinate systems. Figure is reprinted from [8].

In Equations 3.17 and 3.18, m and q are integer numbers at which Fourier-Bessel series are truncated.

Final Equation

Equations 3.9 and 3.16 expresses two relations between **a** and **b** matrices in which **a** and **b** are unknown. By multiplying both sides of equation 3.16 by **S**, **a** can be eliminated and the following equation for **b** is obtained:

$$\mathbf{b_j} - \sum_{\mathrm{l,j}} \mathbf{T_{j,l}}\, \mathbf{b_l} = \mathbf{S}\, \mathbf{Q_j} \tag{3.19}$$

Expanding equation 3.19 for N cylinders results in:

$$\begin{pmatrix} \mathbf{I} & -\mathbf{ST_{1,2}} & -\mathbf{ST_{1,3}} & ... & -\mathbf{ST_{1,N}} \\ -\mathbf{ST_{2,1}} & \mathbf{I} & -\mathbf{ST_{2,3}} & ... & -\mathbf{ST_{2,N}} \\ -\mathbf{ST_{3,1}} & -\mathbf{ST_{3,2}} & \mathbf{I} & ... & -\mathbf{ST_{3,N}} \\ ... & ... & ... & ... & ... \\ -\mathbf{ST_{N,1}} & -\mathbf{ST_{N,2}} & -\mathbf{ST_{N,3}} & ... & \mathbf{I} \end{pmatrix} \times \begin{pmatrix} \mathbf{b_1} \\ \mathbf{b_2} \\ \mathbf{b_3} \\ ... \\ \mathbf{b_N} \end{pmatrix} = \begin{pmatrix} \mathbf{SQ_1} \\ \mathbf{SQ_2} \\ \mathbf{SQ_3} \\ ... \\ \mathbf{SQ_N} \end{pmatrix} \tag{3.20}$$

By solving Equation 3.20, **b** matrices, and accordingly, **a** and **c** matrices can be obtained. The size of this system is $N(2M+1)$ if the Fourier-Bessel series are truncated to $2M+1$ terms (limiting m and q between $+M$ and $-M$).

It can be proved that the total field at point P when it is located at a distance from the cylinders is given by [8, 44]:

$$E_z(P) = E_z^i(P) + \sum_{q \in Z} b_q H_q^{(1)}(k_0 n_{ext} r) \exp(iq\theta) \tag{3.21}$$

where (r, θ) are polar coordinates of P in the xy coordinate system depicted in Figure 3.8 and b_q coefficients are expressed as:

$$b_q = \sum_{j=1,N} \sum_{m \in Z} b_{j,m} \exp(i(m-q)\theta^j) J_{q-m}(k_0 n_{ext} r^j) \tag{3.22}$$

$b_{j,m}$ coefficients are obtained from matrix Equation 3.20.

3.4 Results

To validate the proposed design procedure, design of a photonic crystal lens was considered. The initial PC configuration before optimization was a silica slab ($n =$

1.45) with an embedded hexagonal lattice of silicon cylinders ($n = 3.46$ at $\lambda_0 = 1500$ nm) as shown in Figure 3.9. The total number of cylinders in the initial configuration was 211 and it contained 9 layers along the x-axis. A lattice constant of a, a cylinder radius of $r = 0.294a$, and a working frequency of 0.197 (in units of $2\pi c/a$) below the bandgap of the initial crystal was chosen. This initial crystal property was the same as what is used in [11] in which the problem was solved with genetic algorithms. In our validation, the structure was illuminated with an s-polarized light propagating along the x-axis with similar distribution as given in Equation 3.1.

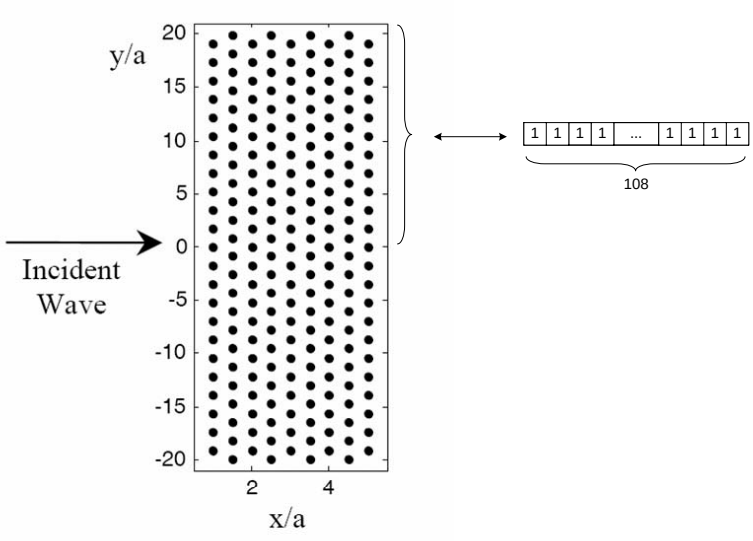

Figure 3.9: Configuration of the initial PC used in the optimization procedure.

The objective of the optimizer was to impose the focal point to be located on the symmetry axis of the lens with $x = 4.6\lambda$, where λ was $a/0.197$. For this purpose, the optimizer was conditioned to search in the space of binary strings in which a PC-based configuration was represented by a string whose bits specify whether the corresponding dielectric cylinders in the configuration should be removed. Due to the structure symmetry, the search space was restricted to symmetrical configurations; this effectively reduced the problem size by 50%.

For a PC-based configuration, the electric field at the desired focal point was

calculated by SMM using Equation 3.21. All Fourier-Bessel series were truncated to 11 terms (m and q were limited between -5 to +5). In each optimization step, after evaluating the characteristics of a PC-based configuration by SMM, its corresponding binary string received a real number fitness to represent the performance of that configuration. The negative logarithm of the electric field modulus in the selected position as the focal point is chosen to provide the fitness of each PC-based configuration by:

$$fitness = -log|E_z(x_{focalpoint}, y_{focalpoint})| \tag{3.23}$$

Boolean PSO was used to minimize the fitness defined in Equation 3.23. This iterative process was continued until there was no improvement of the best fitness value over several iterations.

3.4.1 Photonic Crystal Lens

Figure 3.10 shows the resulting lens and the pattern of corresponding electric field modulus; lighter areas correspond to higher intensities. The edge scattering is due to the plane wave excitation and thus it can be reduced by illuminating the structure with a Gaussian beam and also by considering the points around the edges in the objective function as well. Figure 3.11 shows the x-component of the Poynting vector at a line parallel to y-axis which passes through the focal point. By fitting S_x to a Gaussian function, a beam width of $w_0 = 0.25\lambda_0$ was obtained. Gaussian optics states that the F-number is equal to $2\pi w_0/4\lambda_0$; the F-number of the designed lens was 0.39 which was about 20% better than that reported in [11].

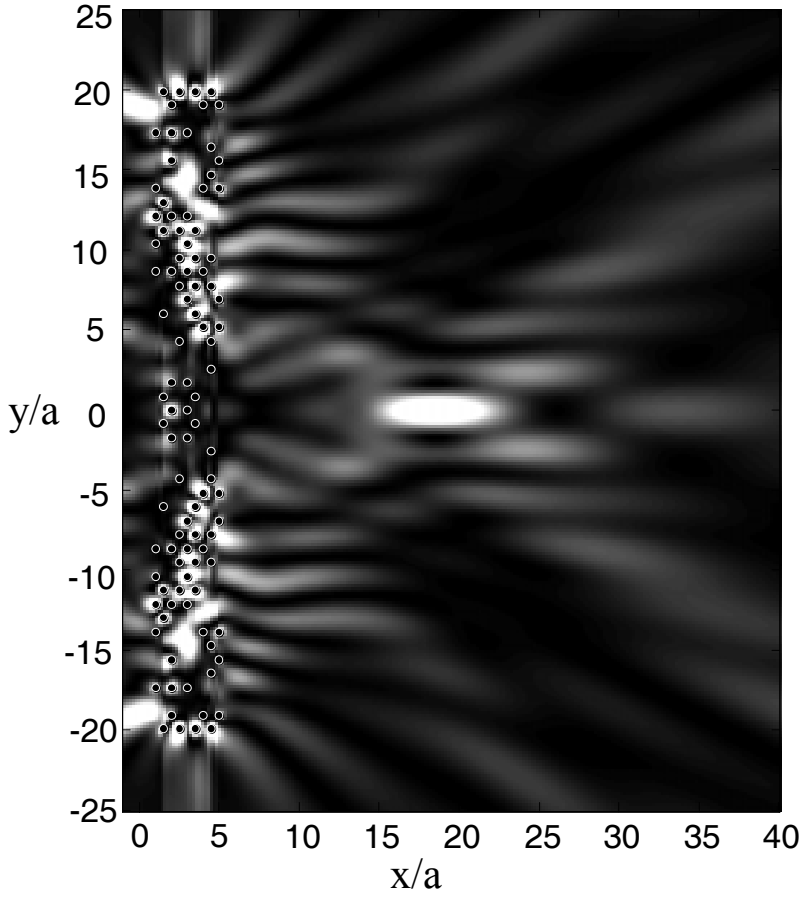

Figure 3.10: Modulus of the electric field distribution produced by the optimized lens.

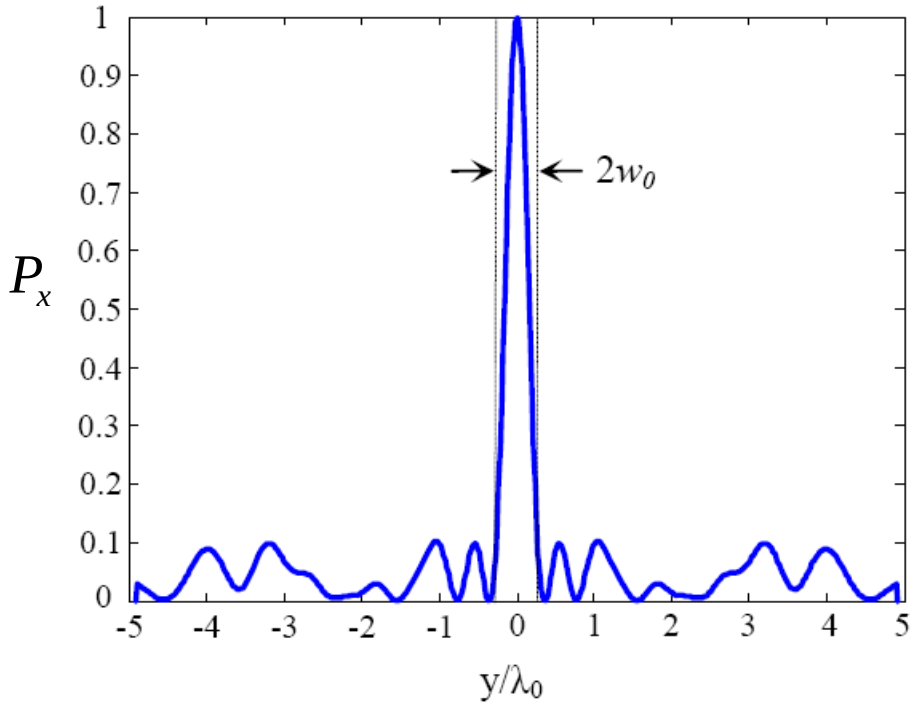

Figure 3.11: The x-component of the Poynting vector along the focal point.

3.4.2 Comparison with Genetic Algorithm

A convergence comparison between Boolean PSO and GA applied to this problem is depicted in Figure 3.12. The population size for both methods was 100. As it can be seen in the figure, although GA was started by a better fitness, it was trapped in a local optimum; however, Boolean PSO found that local optimum earlier and got a better result after a few iterations.

3.5 Conclusions

In this chapter, it was demonstrated that the integration of scattering matrix method with Boolean PSO has promising behavior to solve design problems in the field of photonic crystals. The effectiveness of the proposed method was demonstrated for the optimization problem of a PC-based lens with a low F-number. It has been also

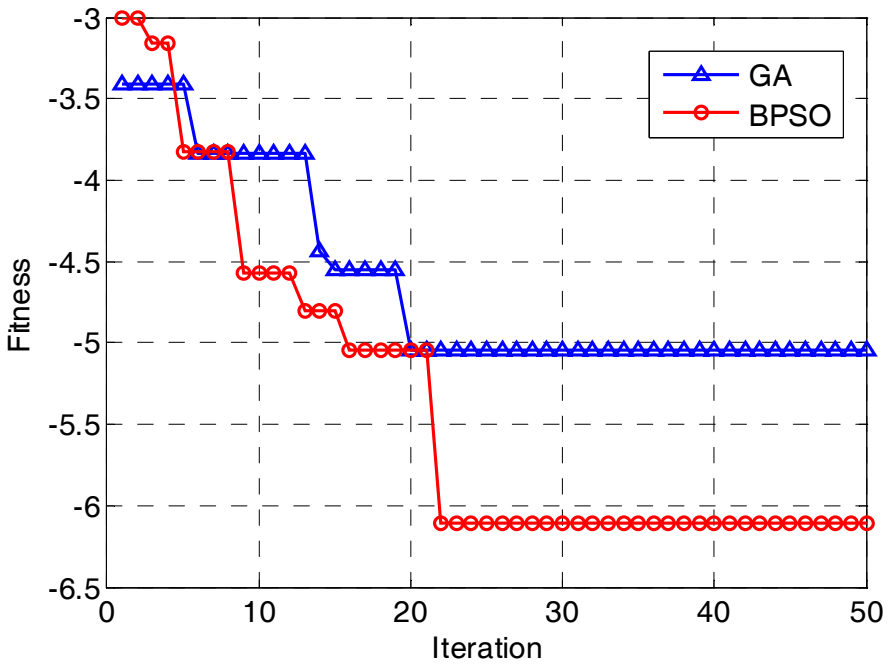

Figure 3.12: Best fitness of iterations in two methods applied to the photonic crystal lens problem (fitness $= -\log|\mathrm{E_z}(\mathrm{x_{focalpoint}}, \mathrm{y_{focalpoint}})|$). Boolean PSO and GA population was 108. Boolean PSO parameters were $C_1 = C_2 = 0.5$ $\Omega = 0.1$ and $V_{max} = 25$. GA crossover rate was 0.8, mutation rate was 0.1. Roulette-wheel selection was used.

shown that the Boolean PSO has a better optimization performance for solving this problem in comparison with GA.

Chapter 4

Design of Binary Supergratings

4.1 Introduction

The binary supergrating (BSG) consists of an aperiodic chain of elements with a fixed length and two allowed refractive index values for each element. These constraints make the BSG well-suited to semiconductor fabrication - requiring only a single lithographic step. So far, the BSG design techniques have been based on Fourier methods which allows for designing BSGs with almost arbitrary wavelength filtering [27]. However, only small refractive index steps are allowed when Fourier methods are used which results in long BSG devices ($\approx$ 1 mm) [27, 47].

In this chapter, we propose the use of a large refractive index step BSG to allow for **compact** optical filters with **near-arbitrary** wavelength filtering that may be readily fabricated with existing photolithography methods. The filters are designed using a combination of Boolean PSO as the optimization technique and a one-dimensional transmission matrix method as the simulation tool. To show the versatility of the proposed method, filters for different applications are considered here. Pass-band filters for wavelength-division multiplexing (WDM) are presented. Several compact wavelength-selective filters with different transmission wavelengths but similar structural parameters are designed. A compact multi-wavelength filter for tunable lasers

is also demonstrated. A broadband filter for intrachip optical networks is proposed as well.

This chapter starts with a brief review of large refractive index step binary supergrating. Then, the proposed method of designing large refractive index BSG is described. Two design cases used to validate the Boolean PSO-based design method is presented after that. For comparison, a genetic algorithm is also used in place of the Boolean PSO. Finally, the designed filters are presented followed by a discussion and conclusion section.

4.2 Large Refractive Index Step Binary Supergrating

Figure 4.1 shows a schematic of the large refractive index step BSG. The light is confined in the transverse plane by an integrated waveguide. A grating is integrated within the waveguide. The light wave is impingent normally upon the grating, as shown in figure 4.1. The incident light wave undergoes partial reflections at the boundaries between elements. The sum of all reflected waves add up to a single backward wave traveling to the left and the sum of all transmitted waves add up to a single forward wave traveling to the right. The refractive indexes, length, and distribution of the elements of the BSG determine the frequency dependency of the backward and forward waves. The BSG structure has frequency selectivity that is useful in many applications.

The grating can be represented by a binary string, where a "1" bit corresponds to the small refractive index and a "0" bit corresponds to the large refractive index. For fixed refractive indexes and element length, different aperiodic sequences or binary strings will have different optical filtering characteristics. Due to the binary nature of the BSG problem, Boolean PSO is used to find the desired sequence of the large

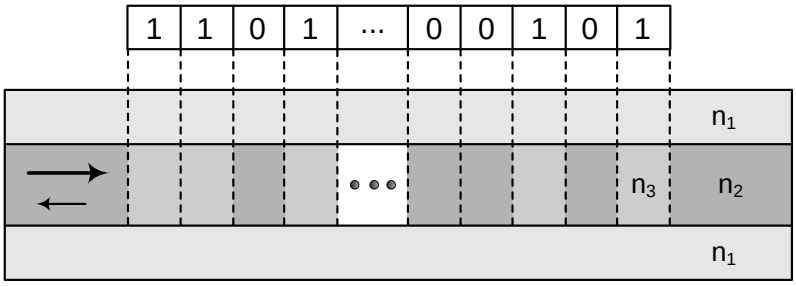

Figure 4.1: A binary super-grating embedded in an optical waveguide ($n_1 < n_3 < n_2$). A binary string is used to represent the refractive index distribution of the binary supergrating. The large arrow shows the incident wave and the small arrow shows the reflected wave.

index step BSG for a desired optical filter which cannot be achieved using past Fourier methods.

4.3 Design Method

Boolean PSO is combined with transmission matrix method to design appropriate binary supergratings without any prior knowledge of possible configurations. The optimization objective is to provide a device with a desired transmittance (or reflectance) spectrum, $T_D(\lambda)$, in the wavelength range of $[\lambda_1, \lambda_2]$. For this purpose, the optimization starts with a set of random binary strings each of them shows a possible BSG configuration. The transmittance spectrum of each candidate BSG, $T_P(\lambda)$, is calculated using transmission matrix method [48]. Details of this method is provided in the next section. The corresponding string to each candidate BSG receives a real number fitness calculated according to its transmittance spectra. Many possible fitness functions can be defined to compute the optimization goal. Here, the summation over absolute differences between the desired transmittance spectra and the candidate transmittance spectra is chosen to provide the fitness of each candidate by:

$$F(P) = \sum_{\lambda} |T_P(\lambda) - T_D(\lambda)| \tag{4.1}$$

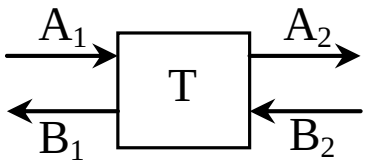

Figure 4.2: Transmission matrix of a two-port network.

After calculating the fitness of all candidates at the first step, the binary strings are updated according to Boolean PSO rules and this process continues until reaching the optimization goal.

4.3.1 Transmission Matrix Method

The transmission matrix method represents the incident and reflected field amplitudes at a given port of a network in terms of those at the other ports [48]. For a two-port network as depicted in Figure 4.2, the transmission matrix is defined as

$$\begin{pmatrix} A_1 \\ B1 \end{pmatrix} = \begin{pmatrix} T_{11} & T_{12} \\ T_{21} & T_{22} \end{pmatrix} \begin{pmatrix} A_2 \\ B_2 \end{pmatrix} \tag{4.2}$$

where the transmission matrix elements are given by:

$$\frac{T_{21}}{T_{11}} = \left.\frac{B_1}{A_1}\right|_{B_2=0} \qquad \frac{1}{T_{11}} = \left.\frac{A_2}{A_1}\right|_{B_2=0} \qquad -\frac{T_{12}}{T_{11}} = \left.\frac{A_2}{B_2}\right|_{A_1=0} \qquad \frac{det\,\mathbf{T}}{T_{11}} = \left.\frac{B_1}{B_2}\right|_{A_1=0} \tag{4.3}$$

The transmission matrix is often used when two-port networks are serially cascaded. The reason is that by simply multiplying the transmission matrices of the individual networks, the fields on the left side of the overall network can be related to the fields on the right side. For example, for the two cascaded networks depicted

in Figure 4.3, this relation is obtained by:

$$\begin{pmatrix} A_1 \\ B1 \end{pmatrix} = \begin{pmatrix} T_{11} & T_{12} \\ T_{21} & T_{22} \end{pmatrix} \begin{pmatrix} A_2 \\ B_2 \end{pmatrix} = \begin{pmatrix} T_{11} & T_{12} \\ T_{21} & T_{22} \end{pmatrix} \begin{pmatrix} T'_{11} & T'_{12} \\ T'_{21} & T'_{22} \end{pmatrix} \begin{pmatrix} A'_2 \\ B'_2 \end{pmatrix} \tag{4.4}$$

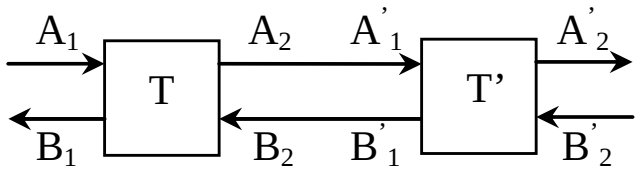

Figure 4.3: Two cascaded networks.

This procedure can be continued to calculate the overall transmission matrix of a chain of two-port networks.

Relation Between Transmission and Scattering Matrices

Equation 4.3 shows that the transmission matrix elements do not directly represent the relations between the incident field amplitude at one port and the reflected field at the same port or the transmitted field through the other port. Scattering matrix is another matrix representation of a network which relates the incident and reflected fields straightforwardly. For the two-port network depicted in Figure 4.4, the scattering matrix is defined as:

$$\begin{pmatrix} b_1 \\ b_2 \end{pmatrix} = \begin{pmatrix} S_{11} & S_{12} \\ S_{21} & S_{22} \end{pmatrix} \begin{pmatrix} a_1 \\ a_2 \end{pmatrix} \tag{4.5}$$

The correspondence between the transmission matrix and scattering matrix amplitudes is as follows: $A_1 = a_1$, $B_1 = b_1$, $A_2 = b_2$ and $B_2 = a_2$.

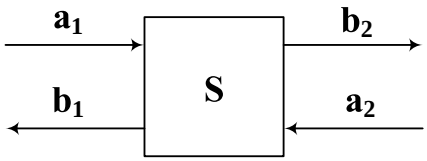

Figure 4.4: Scattering matrix of a two-port network.

The scattering matrix elements are given by:

$$S_{11} = \left.\frac{b_1}{a_1}\right|_{a_2=0} \qquad S_{21} = \left.\frac{b_2}{a_1}\right|_{a_2=0} \qquad S_{22} = \left.\frac{b_2}{a_2}\right|_{a_1=0} \qquad S_{12} = \left.\frac{b_1}{a_2}\right|_{a_1=0} \tag{4.6}$$

Referring to Equation 4.6, it is clear that S_{11} and S_{21} directly express the transmittance and reflectance of a network when it is excited at port one. However, it is not easy to find the overall scattering matrix of a chain of cascaded networks. Consequently, to obtain the transmittance and reflectance of a cascaded network, firstly, the overall transmission matrix is calculated, and secondly, the overall scattering matrix is derived from it using the following matrix equation:

$$\mathbf{S} = \frac{1}{T_{11}} \begin{pmatrix} T_{21} & det\,\mathbf{T} \\ 1 & -T_{12} \end{pmatrix} \tag{4.7}$$

S_{11} and S_{21} of the overall scattering matrix represents the transmittance and reflectance of the cascaded network.

4.3.2 Transmission Matrix Method for Binary Supergratings

For the binary grating shown in Figure 4.5, each element is approximated by a layer with refractive index of n_2 or n_3. The transmission matrix of an element containing

a boundary from n_3 to n_2 and a propagation length of L is given by:

$$T = \frac{1}{t}\begin{pmatrix} e^{j\beta L} & r\,e^{-j\beta L} \\ r\,e^{j\beta L} & e^{-j\beta L} \end{pmatrix} \tag{4.8}$$

where β is the propagation constant of the element with a refractive index of n_2, and r and t are expressed as:

$$r = \frac{n_3 - n_2}{n_3 + n_2} \qquad r^2 + t^2 = 1 \tag{4.9}$$

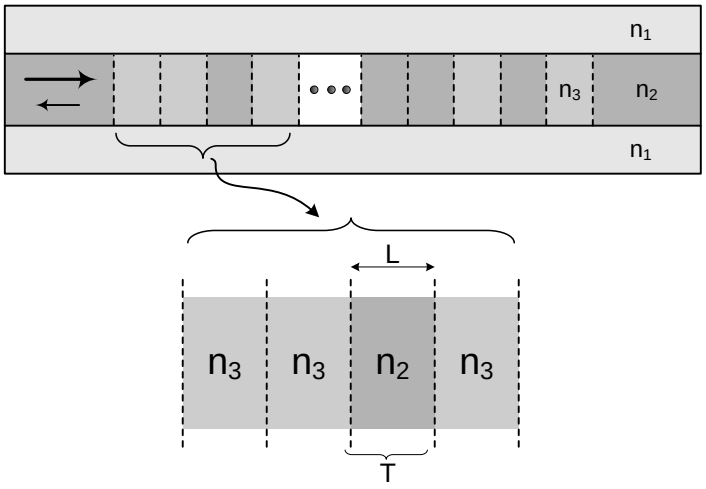

Figure 4.5: Schematic of a binary supergrating in which a set of elements are magnified.

To calculate the transmittance or reflectance of the binary grating at a given wavelength, in the first step, the transmission matrices of its individual elements are multiplied. In the second step, the scattering matrix is calculated using Equation 4.7 in which S_{12} and S_{11} provide the transmittance and reflectance of the grating, respectively.

4.4 Validation of the Method

The Boolean PSO-based design method for the BSG was tested by two design cases. In the first case, the reflectance spectrum of a single defect cavity sandwiched between two Bragg reflectors was provided as the optimization goal. In the second case, the reflectance spectrum of a grating with a random refractive index distribution was considered as the optimization goal. The method was also compared with a genetic algorithm in both cases.

4.4.1 Bragg Reflectors Containing a Single Defect Cavity

In this case, the optimization goal was the reflectance spectrum of a 20 layer Bragg reflector containing a cavity at the middle. The desired device and its corresponding reflectance spectrum are depicted in Figures 4.6 and 4.7. The length of each element was a quarter wavelength in the material where $\lambda_0 = 1550\,\text{nm}$. In the binary array, "0" and "1" represented refractive indexes of 3.5 and 1, correspondingly.

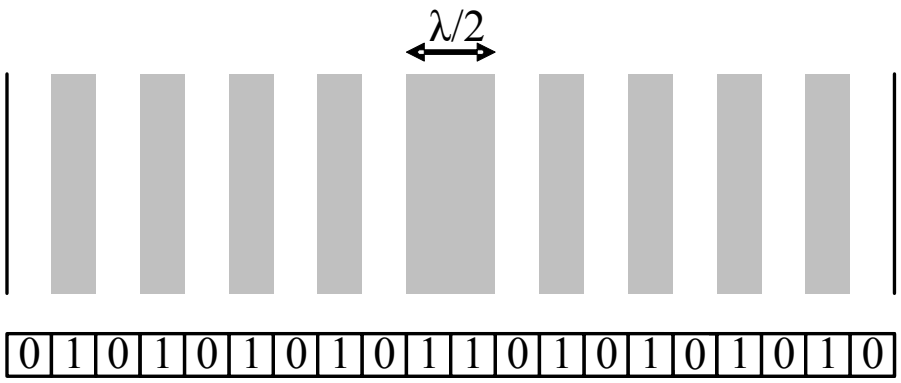

Figure 4.6: A defect cavity sandwitched between two Bragg reflectors with its corresponding binary array.

Starting the optimization with random distributions, the method was able to find the desired test structure in 600 fitness evaluations. We also compared the method

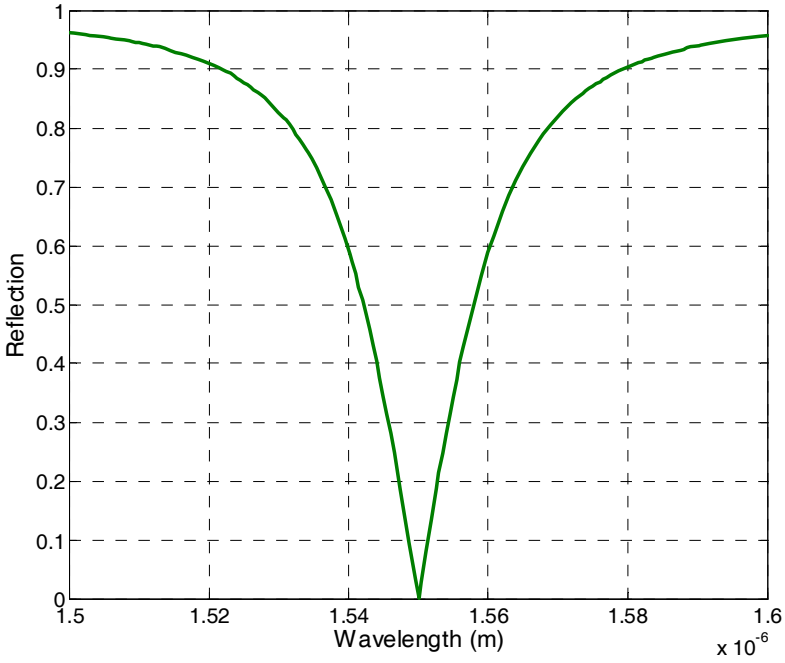

Figure 4.7: The reflectance spectrum of the grating shown in Figure 4.6

with a genetic algorithm which required 800 fitness evaluations to obtain the same result. The behavior of these optimization methods in dealing with this problem is shown in Figure 4.8. This figure shows that this was a very easy problem for both GA and Boolean PSO.

The Boolean PSO efficiency in dealing with arrays with larger sizes was also studied. Here, the objective spectrum was set as before, but the array size is increased. Therefore, the same 20 bit array surrounded by a bunch of zeros was expected as the potential answer of the optimization process. This was a non-polynomial (NP) time problem because the search space size was $2^{ArraySize}$, however, it was expected that Boolean PSO obtain a close to optimum answer in a reasonable time.

Figure 4.9 shows the required time for Booelan PSO to obtain the optimum result for different array sizes with the same objective. For example, the time needed to get an acceptable result for a 100 bit array was around one hour on a workstation

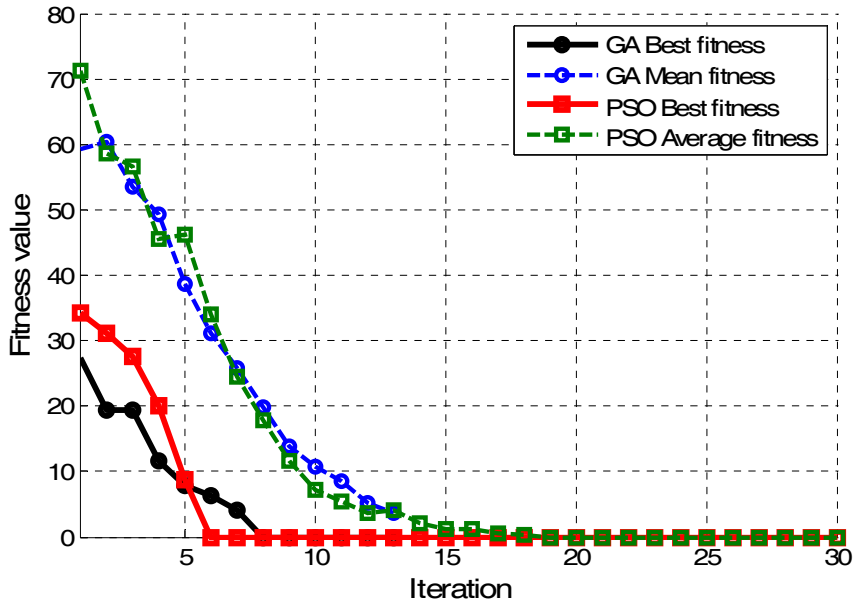

Figure 4.8: The behavior of Boolean PSO and GA in a 20 layer filter design problem. Boolean PSO population was 100, $C_1 = C_2 = 0.5$ $\Omega = 0$ and $V_{max} = 5$. GA population was 100, crossover rate was 0.8, mutation rate was 0.1. Roulette-wheel selection was used.

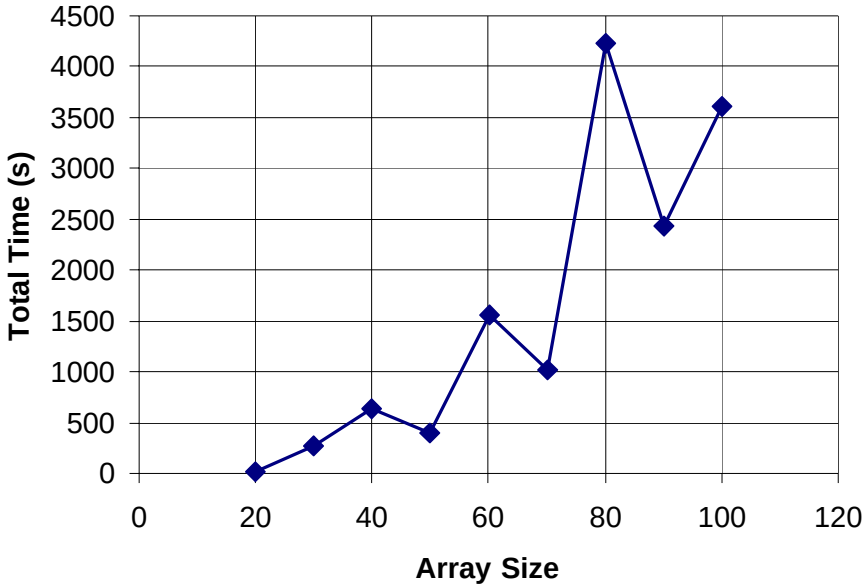

Figure 4.9: Required time for Boolean PSO to obtain the optimum result versus the array size. The population size is $5 \times ArraySize$ and $V_{max} = \frac{ArraySize}{4}$. The simulations are done on a workstation with single core Pentium IV 3GHz CPU, and 4GB of RAM.

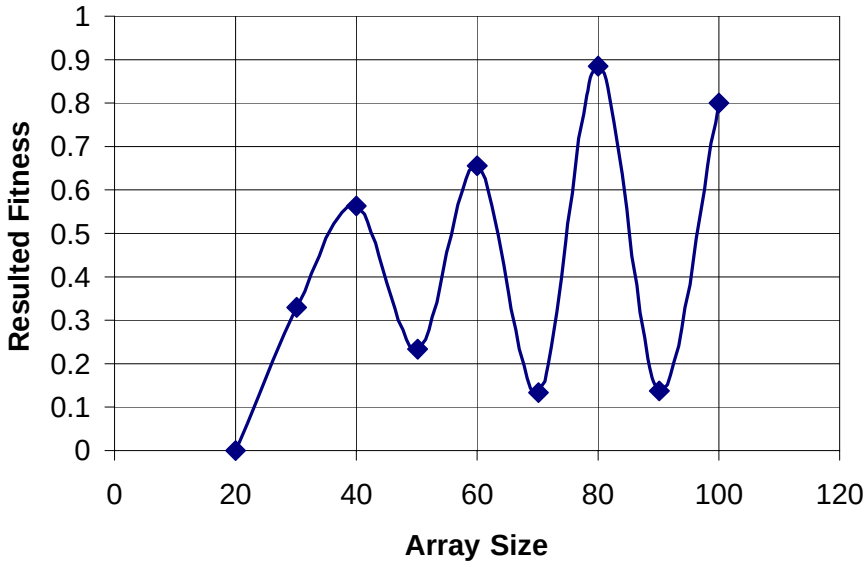

Figure 4.10: The best obtained fitness versus the array size.

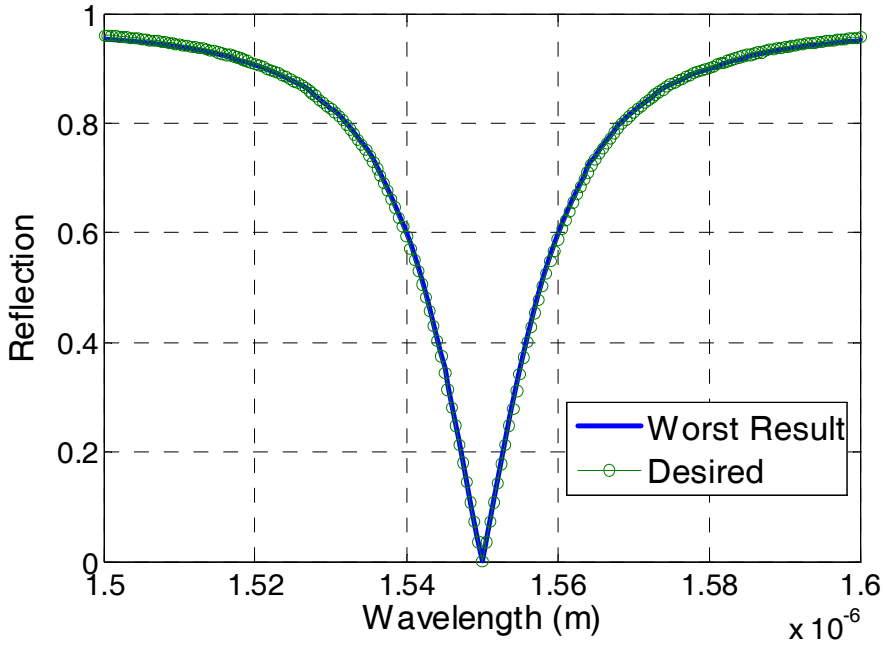

Figure 4.11: The reflection spectrum of the worst obtained result in comparison with the desired spectrum. The array size is 80.

with single core Pentium IV 3GHz CPU, and 4GB of RAM. . The population was five times the array size in each case. As it was shown in Figure 4.9, for arrays larger than 20 bits, the algorithm was not able to find the optimum in a short period of time. The worst fitness was around 0.9 when the given array size was 80 as depicted in Figure 4.10. For this case, the desired and obtained spectra are shown in Figure 4.11. It is obvious that the Boolean PSO result is acceptable, because there is a negligible difference between the spectrum obtained by Boolean PSO and the desired spectrum, even in the worst case. When the array size is large, it is not possible to search the whole space in a reasonable period of time and the close to global optimum result of Boolean PSO is good enough.

4.4.2 BSG with a Random Refractive Index Distribution

To examine the optimizer efficiency in exploring the search space further, another case was considered in which the array did not have a simple distribution of zeros and ones. A 40 bit random array was generated and its spectrum was chosen as the desired spectrum. Figure 4.12 shows the behavior of Boolean PSO and genetic algorithm in dealing with this problem. The population size for both methods were 800. The Boolean PSO reached the global optimum after 10400 simulations (13 iterations). However, GA was not able to find the global optimum and after 16000 simulations (20 iterations) it resulted in a fitness of 0.03.

4.5 Results

By using Boolean PSO in combination with transmission matrix method, BSG filters for four different applications were designed. In all design processes, the Boolean PSO parameter values were 0.1 for the inertia weight (Ω) and 0.5 for acceleration constants (C_1, C_2). In each case, we chose the number of solutions at each iteration

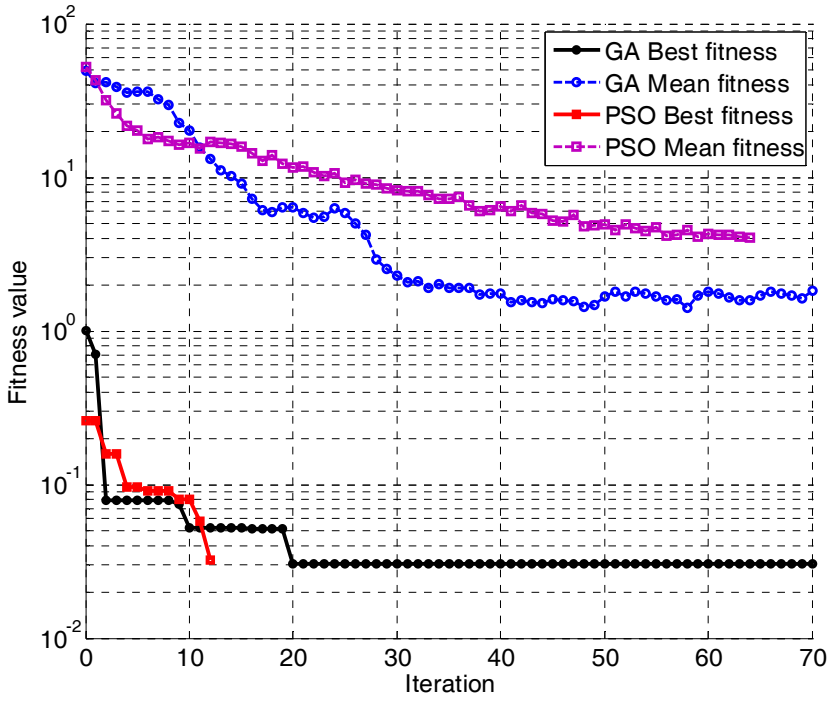

Figure 4.12: The behavior of Boolean PSO and GA in a 40 layer filter design problem. Boolean PSO and GA population was 800, $C_1 = C_2 = 0.5$ $\Omega = 0$ and $V_{max} = 10$. GA crossover rate was 0.8, mutation rate was 0.1. Roulette-wheel selection was used.

equal to the total number of elements in the BSG array. For comparison, we also used a genetic algorithm in place of the Boolean PSO in some design cases.

4.5.1 Pass-Band Filters for Wavelength-Division Multiplexing

Two WDM pass-band filters with maximum transmittance at 1540 and 1550 nm and 0.8 nm bandwidth were designed. Figures 4.13 and 4.14 shows the final transmittance of the optimized filters. The desired transmittance spectrum was 0 dB transmission in the pass-band and below −30 dB outside the pass-band. The length of the elements was a quarter wavelength in the material. For the filter at 1540 nm, the allowed refractive indexes were 3.5 and 2.5, and the total device length was only 79 μm. For the other filter, the total device length was 113 μm and the refractive indexes were 3.2 and 2.7.

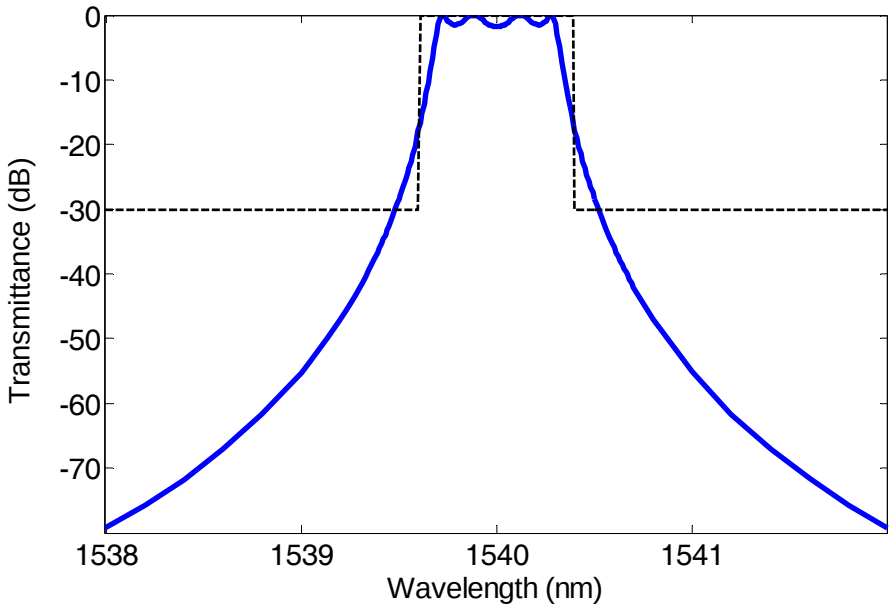

Figure 4.13: Transmittance spectrum of the optimized 79 μm long pass-band filter.

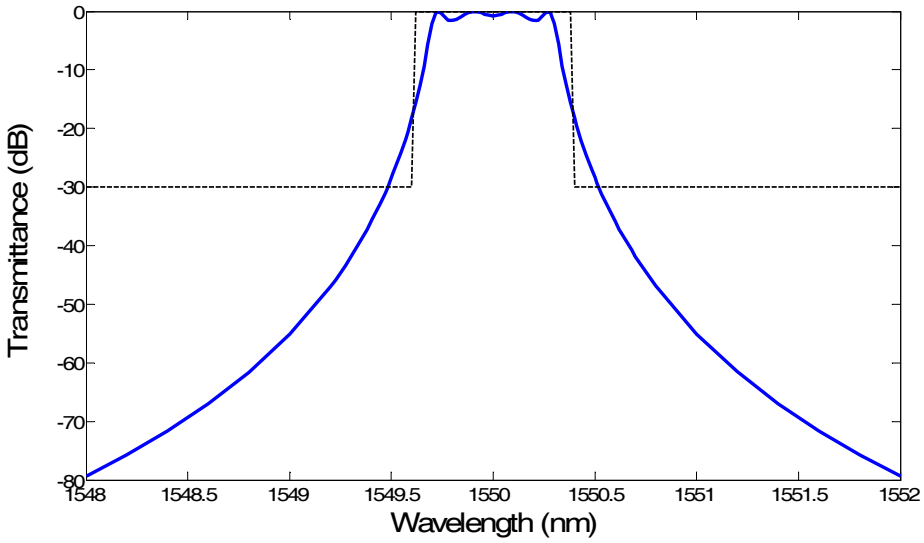

Figure 4.14: Transmittance spectrum of the optimized 113 μm long pass-band filter.

4.5.2 Wavelength-Selective Filters

Here, a series of single-wavelength BSG filters were designed. Each filter had a transmission wavelength that could be selectively varied over 10 nm wavelength range, while all the structural parameters such as element length, number of elements, and refractive index step were maintained. Single-wavelength transmission filters can also be realized by introducing a defect in a photonic crystal structure. Parameters such as the hole diameter and the defect size must be varied with nanometer resolution to accurately vary the transmission wavelength in PC structures [49]. Alternately, the optical properties of PC structures can also be tuned by microfluidics [50]. In the case of BSG, the desired wavelength is selected by finding the correct order for the binary sequence.

Figure 4.15 shows the transmittance spectra of the optimized BSG filters in the wavelength range of $1540 - 1550$ nm with 2 nm peak spacing. The target wavelengths are shown with dashed vertical lines. The optimization goal was to provide maximum transmission at the desired wavelength while minimizing transmission at

other wavelengths with a fitness function defined in equation 4.1. The refractive indexes were 3.5 and 2.7. The element length was 50 nm, which was the same as past works [47]. The number of elements was 1000 and the total length of each filter was 50 μm, accordingly. It is clear that the Boolean PSO was able to achieve good single-wavelength selection over a wide range of wavelengths.

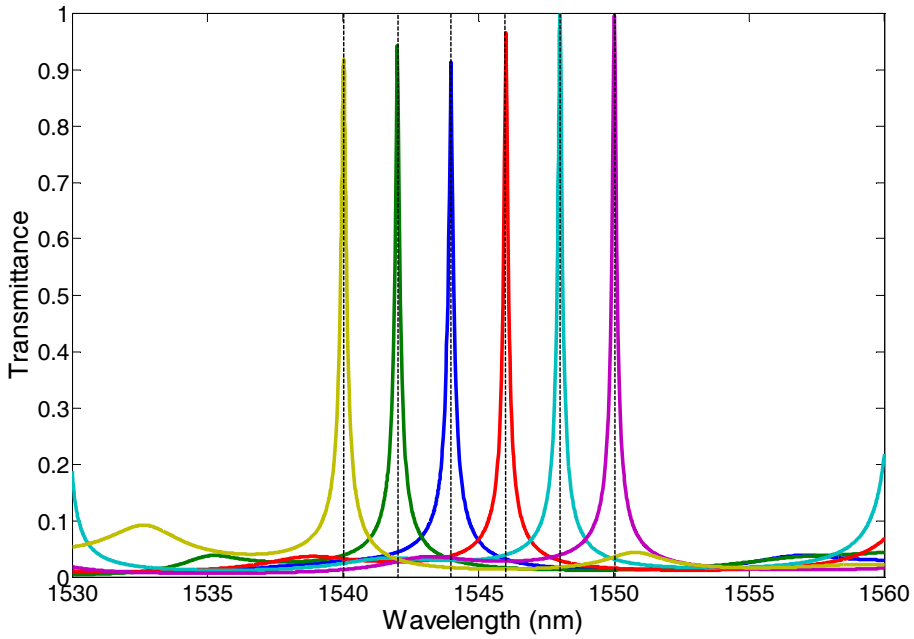

Figure 4.15: Transmittance spectra of 50 μm long BSG filters. The peak spacing is 2 nm.

Figure 4.16 shows the refractive index distribution of the optimized BSG filter at 1550 nm, with the transmission shown in Figure 4.15. A blown-up portion of this distribution is shown to emphasize the aperiodic nature of the optimized BSG structure.

4.5.3 A Multi-Wavelength Filter for Compact Tunable Lasers

In this section, a multi-wavelength filter with three equally spaced peaks of equal transmission is presented. The wavelength spacing was chosen to be 4 nm, as in

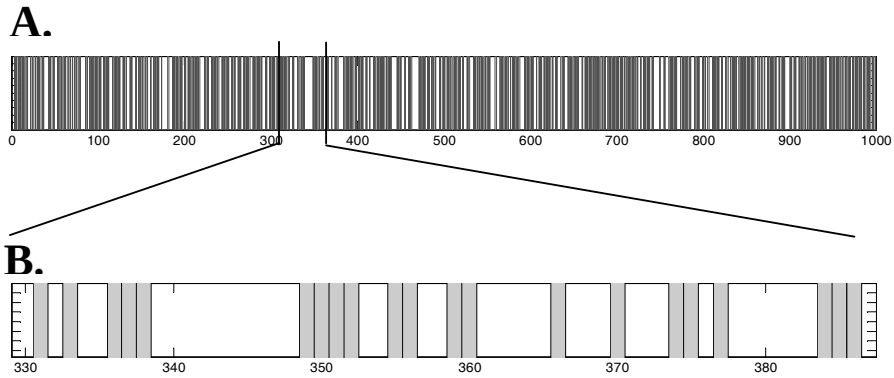

Figure 4.16: **A**. Refractive index distribution of the BSG filter at 1550 nm with 1000 elements. Small refractive index is shown with a dark color bar and large refractive index with a light color bar. **B**. A magnified region of refractive index distribution in part A.

past works on filters for tunable lasers [51]. Here, the element length was doubled to 100 nm (as compared with the single-wavelength filter) to enable less demanding fabrication resolution. It was desirable to maintain a compact design, at least below 100 μm. Therefore, the number of elements was reduced to 800, so that the overall length was 80 μm. The corresponding size of the search space was 2^{800}. The refractive indexes were chosen to be 3.5 and 2.5.

In this case, the optimization of Equation 4.1 had three times the number of wavelengths as the previous example. Therefore, computation time was increased considerably. As a result, we added an ad-hoc penalty to the fitness defined in Equation 4.1 to wean initial poor candidates from the search space.

Figure 4.17 shows the results for the calculated transmittance spectrum of the optimized BSG.

4.5.4 A Broad-Band Filter for Intarchip Optical Networks

Microprocessor performance has been improved recently by using multiple processor cores on a single chip rather than by increasing the transistor speed [52]. Efficient

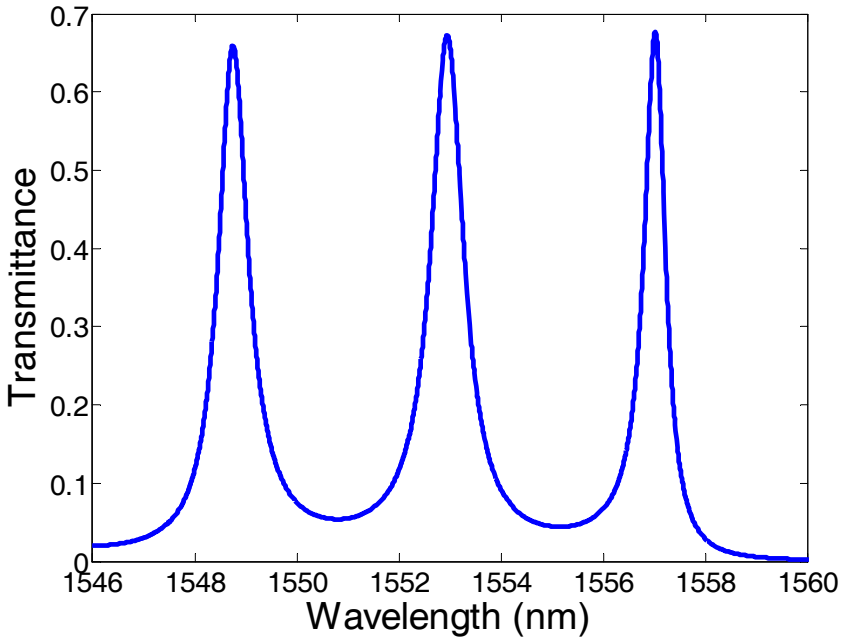

Figure 4.17: Transmittance spectrum of an 80 μm long multi-wavelength BSG filter.

communication among these cores requires ultra-high bandwidths, minimum latencies, and low power dissipation which are not accessible by electrical communications [53, 54]. To avoid the aforementioned bottlenecks in electrical communications, an intrachip optical network (ICON) architecture has been proposed recently [53]. ICON uses 3D integration [55] to combine an on-chip optical network plane with a separate microprocessor plane. Optical components with enormous bandwidths and small footprints are key requirements of ICON.

By using Boolean PSO, a pass-band filter at 1550 nm with a 4 nm bandwidth was designed for ICON applications. Figure 4.18 shows the final transmittance of the optimized filter. Complete transmission in the pass-band and zero transmission outside the pass-band was the desired transmittance spectrum. The basic array was chosen to have 700 elements. The element length was 100 nm and thus the total length of the device was 70 μm. The refractive indexes were chosen to be 3.3 and

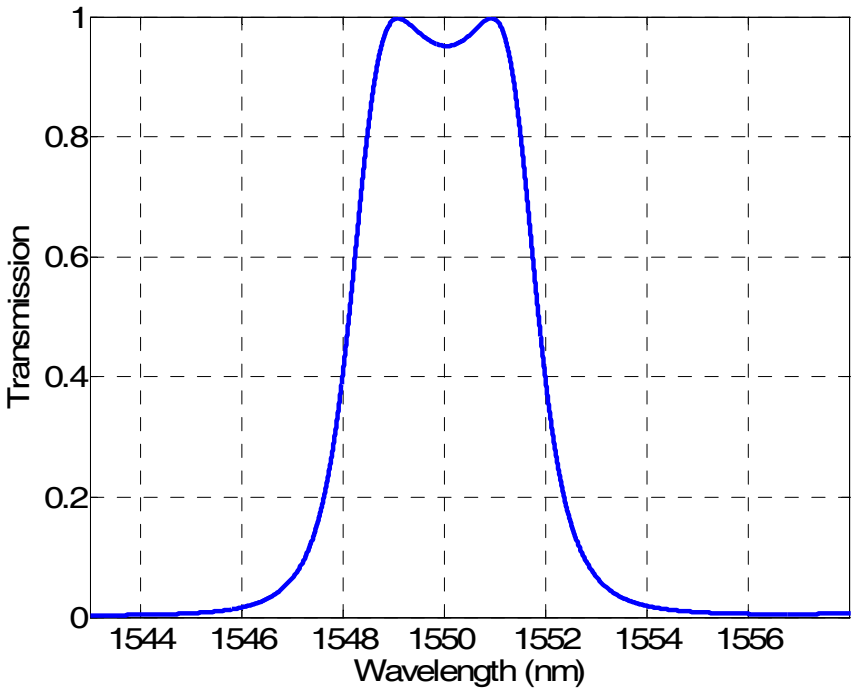

Figure 4.18: Transmittance spectrum of a 70 μm long pass-band BSG filter.

2.6.

The enormous bandwidth and small footprint of this filter makes it appropriate for intrachip optical networks.

4.5.5 Comparison with Genetic Algorithm

We compared the performance of the Boolean PSO with GA in two of the above problems. Figure 4.19 shows the results for the problem of multi-wavelength filter which was the hardest problem for an optimization algorithm due to the number of involved wavelengths. The Boolean PSO converged to a better result in a short time, while the GA was trapped in a poorer local optimum solution. Similar results obtained for the single-wavelength filters. Although in some cases both algorithms result in good solutions, the simpler implementation and reduced bookkeeping of PSO make it appealing [41].

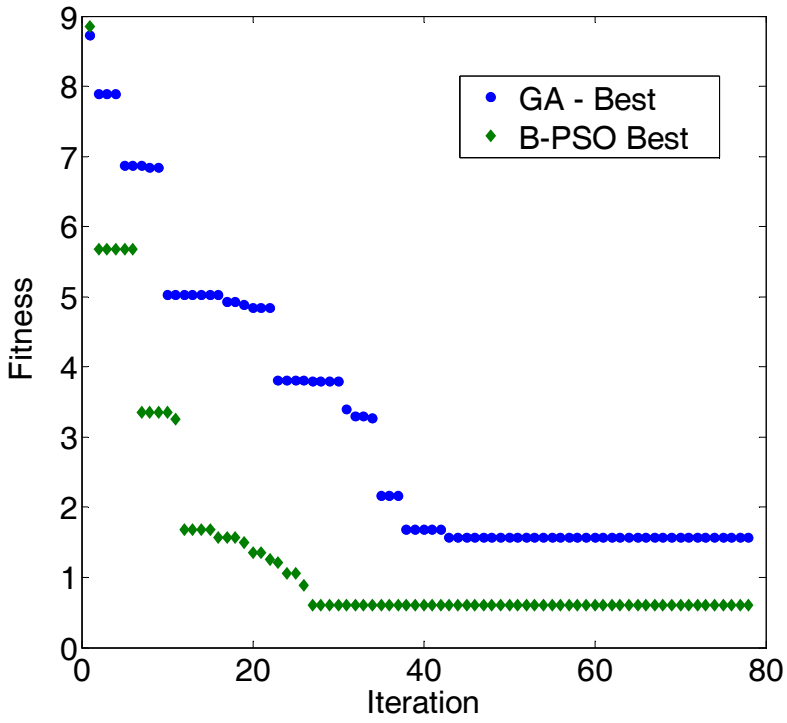

Figure 4.19: Best fitness of iterations in two methods applied to the multi-wavelength BSG of figure 4.17. The Boolean PSO and GA population was equal to the total number of elements in the BSG array. A multipoint crossover GA with a crossover rate of 0.8, a mutation rate of 0.1, and a roulette-wheel selection was used. Boolean PSO parameters were $C_1 = C_2 = 0.5$ $\Omega = 0.1$ and $V_{max} = \frac{ArraySize}{4}$.

4.6 Discussions

The details of BSG implementation depend upon the specific material system used - a tunable laser will likely use active semiconductor materials, whereas an intrachip optical network will likely use silicon-based materials. Here, we did not wish to limit the consideration to a specific implementation, so the problems were considered in one dimension, as was done in the past [27, 47], with the understanding that diffraction losses should be minimized.

As demonstrated in Figure 4.17, the large refractive index step BSG provides multi-wavelength filters that are an order of magnitude more compact than past

multi-wavelength gratings in integrated tunable laser technologies [47, 2]. As compared with single-wavelength photonic crystal filters, the large refractive index step BSG has relaxed resolution, which allows for single-step photolithography, while retain a compact structure.

It should be noted that the desired filter may not exist within the search space provided by the large refractive index step BSG, and so we only claim near-arbitrary filtering capability. While the phase was not included in the fitness function defined in Equation 4.1, it may be modified in a straightforward way to include phase filtering as well.

We have compared the performance of the Boolean PSO with GA in above problems. Although in many cases both algorithms result in good solutions, the simpler understanding and implementation of PSO due to less operators involved in this algorithm make it appealing [41]. Past works have demonstrated Convergence Guaranteed PSO (CGPSO) [56, 57], which may be used to further improve the performance of the compact optical filters proposed here.

4.7 Conclusions

Compact optical filters were demonstrated by using a large refractive index step BSG structure. Combining Boolean particle swarm optimization with the transmission matrix method, pass-band filters for wavelength-division multiplexing applications were designed. Wavelength selection in single wavelength filters was also demonstrated without changing the refractive index step or element length. A multi-wavelength filter which is an order of magnitude shorter than previous BSG devices has also been presented for tunable laser applications. A broad-band filter suitable for intrachip optical networks was also proposed.

The BSG architecture may be readily fabricated with optical lithography and existing semiconductor technology. As compared with defect-based photonic crystal filters, a less stringent fabrication resolution is allowed by the compact large index step BSG, while the device size is still of the order of tens of micrometers. The large refractive index step BSG allows for compact devices that can be densely integrated, which is promising for many applications, including intrachip optical networks and compact tunable lasers.

Chapter 5

Conclusion

The contributions in this thesis are in two areas: (1) developing a new inverse design method for designing two-dimensional photonic crystals, and (2) introducing the concept of binary supergrating with large refractive index changes accompanied by developing an inverse design method for BSG structures.

This thesis introduces Boolean PSO in conjunction with the scattering matrix method as a new tool for designing two-dimensional photonic crystals. The potential of this approach is illustrated in a lens design problem. The PC lens can be used to connect a photonic crystal circuit to an optical fiber. The resulted lens has an F-number of 0.39 which is lower than what is reported so far. The appropriate behavior of this optimization process in comparison with genetic algorithm is also presented.

This thesis also introduces a combination of Boolean particle swarm optimization with the transmission matrix method as a new tool for designing binary supergrating filters with a large refractive index step. This method provides new capability for designing filters with almost arbitrary wavelength filtering and more compact than similar devices previously realized. The versatility of the large refractive index step BSG has been demonstrated by designing filters for various applications. Two WDM pass-band filters with 79 μm and 113 μm lengths are designed to operate at 1540 nm and 1550 nm, respectively. Several 50 μm long single-wavelength filters are designed,

each having a different wavelength while using the same structural parameters. A multi-wavelength filter for tunable lasers is also proposed in an 80 μm long structure. A 70 μm long broad-band filter to operate at 1550 nm is also demonstrated for intrachip optical network applications. A genetic algorithm is substituted for the Boolean PSO; however, Boolean PSO shows better performance in these cases. The BSG architecture may be readily fabricated with optical lithography and existing semiconductor technology, which makes these results exciting for many applications including what is mentioned above. The compact size of the large refractive index step BSG means that it is well-suited for integration, as well as for increasing the number of discrete devices that can be fabricated from a single wafer.

One major enhancement could be made to improve the utility of the proposed inverse design methods if parallel computers are used. In the case of photonic crystal lens, we could only consider the electric field at the focal point due the limited computational resources. Considering more points around the focal point during the optimization might result in a lens with even lower F-number. Although scattering matrix method is a semi-analytical technique and it is fast, adding only one more point around the focal point doubles the optimization time. If parallel computers are not used, the algorithm cannot converge to a solution in a reasonable time period.

In the case of binary supergrating filters especially the multi-wavelength filter, we were not able to extend it to a larger wavelength interval for more peaks. Adding more wavelength samples requires increasingly more time. Parallel computers can open the way for exploring new filters for many applications such as widely tunable lasers.

Bibliography

[1] J. S. Foresi, P. R. Villeneuve, J. Ferrera, E. R. Thoen, G. Steinmeyer, S. Fan, J. D. Joannopoulos, L. C. Kimerling, H. I. Smith, and E. P. Ippen, "Photonic-bandgap microcavities in optical waveguides," *Nature*, vol. 390, pp. 143–145, 1997.

[2] A. Ward, D. Robbins, G. Busico, E. Barton, L. Ponnampalam, J. Duck, N. Whitbread, P. Williams, D. Reid, A. Carter, and M. Wale, "Widely tunable ds-dbr laser with monolithically integrated soa: design and performance," *IEEE Journal of Selected Topics in Quantum Electronics*, vol. 11, no. 1, pp. 149–156, 2005.

[3] D. W. Prather, S. Shi, J. Murakowski, G. J. Schneider, A. Sharkawy, C. Chen, and B. Miao, "Photonic crystal structures and applications: Perspective, overview, and development," *IEEE Journal of Selected Topics in Quantum Electronics*, vol. 12, no. 6, pp. 1416–1437, 2006.

[4] S. Noda, "Recent progresses and future prospects of two- and three-dimensional photonic crystals," *Journal of Lightwave Technology*, vol. 24, no. 12, pp. 4554–4567, 2006.

[5] F. Poletti, V. Finazzi, T. M. Monro, N. G. R. Broderick, V. Tse, and D. J. Richardson, "Inverse design and fabrication tolerances of ultra-flattened dispersion holey fibers," *Opt. Express*, vol. 13, no. 10, pp. 3728–3736, 2005.

[6] P. Borel, A. Harpøth, L. Frandsen, M. Kristensen, P. Shi, J. Jensen, and O. Sig-

mund, "Topology optimization and fabrication of photonic crystal structures," *Opt. Express*, vol. 12, no. 9, pp. 1996–2001, 2004.

[7] A. Håkansson and J. Sánchez-Dehesa, "Inverse designed photonic crystal demultiplex waveguide coupler," *Opt. Express*, vol. 13, no. 14, pp. 5440–5449, 2005.

[8] K. Yasumoto, *Electromagnetic Theory and Applications for Photonic Crystals*. Taylor and Francis Group, 2005.

[9] J. Robinson and Y. Rahmat-Samii, "Particle swarm optimization in electromagnetics," *IEEE Transactions on Antennas and Propagation*, vol. 52, no. 2, pp. 397–407, 2004.

[10] N. Jin and Y. Rahmat-Samii, "Parallel particle swarm optimization and finite-difference time-domain (pso/fdtd) algorithm for multiband and wide-band patch antenna designs," *IEEE Transactions on Antennas and Propagation*, vol. 53, no. 11, pp. 3459–3468, 2005.

[11] A. Hakansson, J. Sanchez-Dehesa, and L. Sanchis, "Inverse design of photonic crystal devices," *IEEE Journal on Selected Areas in Communications*, vol. 23, no. 7, pp. 1365–1371, 2005.

[12] T. Back and H.-P. Schwefel, "Evolutionary computation: an overview," *Proceedings of IEEE International Conference on Evolutionary Computation*, pp. 20–29, May 1996.

[13] J. Kennedy and R. Eberhart, "Particle swarm optimization," *IEEE International Conference on Neural Networks*, vol. 4, pp. 1942–1948 vol.4, November/December 1995.

[14] J. H. Holland, "Genetic algorithms," *Scientific American*, pp. 66–72, 1992.

[15] R. L. Haupt and S. E. Haupt, *Practical Genetic Algorithms*. New York: Wiley, 1998.

[16] Eberhart and Y. Shi, "Particle swarm optimization: developments, applications and resources," *Proceedings of the 2001 Congress on Evolutionary Computation*, vol. 1, pp. 81–86, 2001.

[17] D. Weile and E. Michielssen, "Genetic algorithm optimization applied to electromagnetics: a review," *IEEE Transactions on Antennas and Propagation*, vol. 45, no. 3, pp. 343–353, 1997.

[18] J. Goh, I. Fushman, D. Englund, and J. Vučković, "Genetic optimization of photonic bandgap structures," *Opt. Express*, vol. 15, no. 13, pp. 8218–8230, 2007.

[19] S. Baskar, R. Zheng, A. Alphones, N. Ngo, and P. Suganthan, "Particle swarm optimization for the design of low-dispersion fiber bragg gratings," *IEEE Photonics Technology Letters*, vol. 17, no. 3, pp. 615–617, 2005.

[20] A. Marandi, F. Afshinmanesh, M. Shahabadi, and F. Bahrami, "Boolean particle swarm optimization and its application to the design of a dual-band dual-polarized planar antenna," *IEEE Congress on Evolutionary Computation, CEC 2006*, pp. 3212–3218, July 2006.

[21] F. Afshinmanesh, A. Marandi, and A. Rahimi-Kian, "A novel binary particle swarm optimization method using artificial immune system," *The International Conference on Computer as a Tool, EUROCON 2005*, vol. 1, pp. 217–220, 2005.

[22] C. Manolatou, S. Johnson, S. Fan, P. Villeneuve, H. Haus, and J. Joannopoulos, "High-density integrated optics," *Journal of Lightwave Technology*, vol. 17, no. 9, pp. 1682–1692, 1999.

[23] E. Centeno, B. Guizal, and D. Felbacq, "Multiplexing and demultiplexing with photonic crystals," *Journal of Optics A: Pure and Applied Optics*, pp. L10–L13, 1999.

[24] J. Smajic, C. Hafner, and D. Erni, "Optimization of photonic crystal structures," *J. Opt. Soc. Am. A*, vol. 21, no. 11, pp. 2223–2232, 2004.

[25] A. Mekis, J. C. Chen, I. Kurland, S. Fan, P. R. Villeneuve, and J. D. Joannopoulos, "High transmission through sharp bends in photonic crystal waveguides," *Phys. Rev. Lett.*, vol. 77, no. 18, pp. 3787–3790, 1996.

[26] M. Loncar, T. Yoshie, A. Scherer, P. Gogna, and Y. Qiu, "Low-threshold photonic crystal laser," *Applied Physics Letters*, vol. 81, no. 15, pp. 2680–2682, 2002.

[27] D. Levner, M. Fay, and J. Xu, "Programmable spectral design using a simple binary bragg-diffractive structure," *IEEE Journal of Quantum Electronics*, vol. 42, no. 4, pp. 410–417, 2006.

[28] M.-P. Song and G.-C. Gu, "Research on particle swarm optimization: a review," *Proceedings of 2004 International Conference on Machine Learning and Cybernetics*, vol. 4, pp. 2236–2241 vol.4, August 2004.

[29] M. Khanesar, M. Teshnehlab, and M. Shoorehdeli, "A novel binary particle swarm optimization," *Mediterranean Conference on Control and Automation, MED 07.*, pp. 1–6, June 2007.

[30] F. Afshinmanesh, A. Marandi, and M. Shahabadi, "Design of a single-feed dual-band dual-polarized printed microstrip antenna using a boolean particle swarm optimization," *IEEE Transactions on Antennas and Propagation*, vol. 56, no. 7, pp. 1845–1852, 2008.

[31] F. Afshinmanesh, A. Marandi, P. P. M. So, and R. Gordon, "Proposal for compact optical filters using large index step binary supergratings," *IEEE Photonics Technology Letters*, vol. 20, no. 9, pp. 676–678, 2008.

[32] F. Afshinmanesh, A. Marandi, P. So, and R. Gordon, "Compact binary supergratings using a large refractive index step," *The 20th Annual Meeting of the IEEE Lasers and Electro-Optics Society, LEOS 2007.*, pp. 658–659, October 2007.

[33] Z. D. Zaharis, "Boolean particle swarm optimization of 3-branch gsm/dcs/umts current dividers by using artificial immune system," *IEICE Electronics Express*, vol. 5, no. 2, pp. 41–47, 2008.

[34] A. Marandi, F. Afshinmanesh, and P. So, "Design of a highly focused photonic crystal lens using boolean particle swarm optimization," *The 20th Annual Meeting of the IEEE Lasers and Electro-Optics Society, LEOS 2007*, pp. 931–932, October 2007.

[35] Y.-L. Zheng, L.-H. Ma, L.-Y. Zhang, and J.-X. Qian, "On the convergence analysis and parameter selection in particle swarm optimization," *International Conference on Machine Learning and Cybernetics*, vol. 3, pp. 1802–1807, November 2003.

[36] M. Clerc and J. Kennedy, "The particle swarm - explosion, stability, and convergence in a multidimensional complex space," *IEEE Transactions on Evolutionary Computation*, vol. 6, no. 1, pp. 58–73, 2002.

[37] J. Kennedy and R. Eberhart, "A discrete binary version of the particle swarm algorithm," *IEEE International Conference on Systems, Man, and Cybernetics*, vol. 5, pp. 4104–4108, October 1997.

[38] T. Ting, M. Rao, and C. Loo, "A novel approach for unit commitment problem via an effective hybrid particle swarm optimization," *IEEE Transactions on Power Systems*, vol. 21, no. 1, pp. 411–418, 2006.

[39] J. H. Holland, *Adaption in Natural and Artificial System.* Ann Arbor: The University of Michigan Press, 1975.

[40] J. Johnson and V. Rahmat-Samii, "Genetic algorithms in engineering electromagnetics," *IEEE Antennas and Propagation Magazine*, vol. 39, no. 4, pp. 7–21, 1997.

[41] D. Boeringer and D. Werner, "Particle swarm optimization versus genetic algorithms for phased array synthesis," *IEEE Transactions on Antennas and Propagation*, vol. 52, no. 3, pp. 771–779, 2004.

[42] T. Krauss and R. De La Rue, "Photonic crystals in the optical regime - past, present and future," *Progress in Quantum Electronics*, vol. 23, pp. 51–96, 1999.

[43] G. Tayeb and D. Maystre, "Rigorous theoretical study of finite-size two-dimensional photonic crystals doped by microcavities," *J. Opt. Soc. Am. A*, vol. 14, no. 12, pp. 3323–3332, 1997.

[44] D. Felbacq, G. Tayeb, and D. Maystre, "Scattering by a random set of parallel cylinders," *J. Opt. Soc. Am. A*, vol. 11, no. 9, pp. 2526–2538, 1994.

[45] E. Centeno and D. Felbacq, "Rigorous vector diffraction of electromagnetic waves by bidimensional photonic crystals," *J. Opt. Soc. Am. A*, vol. 17, no. 2, pp. 320–327, 2000.

[46] M. Abramovitz and I. Stegun, *Handbook of Mathematical Functions.* Dover Publications, New York, 1970.

[47] I. Avrutsky, D. Ellis, A. Tager, H. Anis, and J. Xu, "Design of widely tunable semiconductor lasers and the concept of binary superimposed gratings (bsg's)," *IEEE Journal of Quantum Electronics*, vol. 34, no. 4, pp. 729–741, 1998.

[48] L. A. Coldren and S. W. Corzine, *Diode Lasers and Photonic Integrated Circuits*. John Wiley and Sons, 1995.

[49] D. Ripin, K.-Y. Lim, G. Petrich, P. Villeneuve, S. Fan, E. Thoen, J. Joannopoulos, E. Ippen, and L. Kolodziejski, "One-dimensional photonic bandgap microcavities for strong optical confinement in gaas and gaas/alxoy semiconductor waveguides," *Journal of Lightwave Technology*, vol. 17, no. 11, pp. 2152–2160, 1999.

[50] A. Sharkawy, D. Pustai, S. Shi, D. Prather, S. McBride, and P. Zanzucchi, "Modulating dispersion properties of low index photonic crystal structures using microfluidics," *Opt. Express*, vol. 13, no. 8, pp. 2814–2827, 2005.

[51] B. Mason, S. DenBaars, and L. Coldren, "Tunable sampled-grating dbr lasers with integrated wavelength monitors," *IEEE Photonics Technology Letters*, vol. 10, no. 8, pp. 1085–1087, 1998.

[52] V. Agarwal, M. Hrishikesh, S. Keckler, and D. Burger, "Clock rate versus ipc: the end of the road for conventional microarchitectures," *Proceedings of the 27th International Symposium on Computer Architecture*, pp. 248–259, 2000.

[53] J. Kash, "Intrachip optical networks for a future supercomputer-on-a-chip," *Photonics in Switching*, pp. 55–56, August 2007.

[54] R. Ho, K. Mai, and M. Horowitz, "The future of wires," *Proceedings of the IEEE*, vol. 89, no. 4, pp. 490–504, 2001.

[55] M. Ieong, K. Guarini, V. Chan, K. Bernstein, R. Joshi, J. Kedzierski, and W. Haensch, "Three dimensional cmos devices and integrated circuits," *Proceedings of the IEEE 2003 Custom Integrated Circuits Conference*, pp. 207–213, September 2003.

[56] J. Sun, W. Xu, and B. Feng, "Adaptive parameter control for quantum-behaved particle swarm optimization on individual level," *IEEE International Conference on Systems, Man and Cybernetics*, vol. 4, pp. 3049–3054, October 2005.

[57] X. Chen and Y. Li, "A modified pso structure resulting in high exploration ability with convergence guaranteed," *IEEE Transactions on Systems, Man, and Cybernetics, Part B*, vol. 37, no. 5, pp. 1271–1289, 2007.